

# MIKE 21 & MIKE 3 Flow Model FM

Mud Transport Module

Scientific Documentation



**DHI A/S headquarters**

Agern Allé 5  
DK-2970 Hørsholm  
Denmark

+45 4516 9200 Telephone

[mike@dhigroup.com](mailto:mike@dhigroup.com)

[www.mikepoweredbydhi.com](http://www.mikepoweredbydhi.com)

Company Registration No.: DK36466871

## PLEASE NOTE

### **COPYRIGHT**

This document refers to proprietary computer software, which is protected by copyright. All rights are reserved. Copying or other reproduction of this manual or the related programmes is prohibited without prior written consent of DHI. For details please refer to your 'DHI Software Licence Agreement'.

### **LIMITED LIABILITY**

The liability of DHI is limited as specified in your DHI Software License Agreement:

In no event shall DHI or its representatives (agents and suppliers) be liable for any damages whatsoever including, without limitation, special, indirect, incidental or consequential damages or damages for loss of business profits or savings, business interruption, loss of business information or other pecuniary loss arising in connection with the Agreement, e.g. out of Licensee's use of or the inability to use the Software, even if DHI has been advised of the possibility of such damages.

This limitation shall apply to claims of personal injury to the extent permitted by law. Some jurisdictions do not allow the exclusion or limitation of liability for consequential, special, indirect, incidental damages and, accordingly, some portions of these limitations may not apply.

Notwithstanding the above, DHI's total liability (whether in contract, tort, including negligence, or otherwise) under or in connection with the Agreement shall in aggregate during the term not exceed the lesser of EUR 10.000 or the fees paid by Licensee under the Agreement during the 12 months' period previous to the event giving rise to a claim.

Licensee acknowledge that the liability limitations and exclusions set out in the Agreement reflect the allocation of risk negotiated and agreed by the parties and that DHI would not enter into the Agreement without these limitations and exclusions on its liability. These limitations and exclusions will apply notwithstanding any failure of essential purpose of any limited remedy.

# CONTENTS

## MIKE 21 & MIKE 3 Flow Model FM Mud Transport Module Scientific Documentation

<b>1</b>	<b>Introduction .....</b>	<b>1</b>
<b>2</b>	<b>What is Mud .....</b>	<b>2</b>
<b>3</b>	<b>General Model Description .....</b>	<b>3</b>
3.1	Introduction .....	3
3.2	Governing Equations 2D .....	4
3.3	Numerical Schemes .....	4
<b>4</b>	<b>Cohesive Sediments .....</b>	<b>6</b>
4.1	Introduction .....	6
4.2	Deposition .....	7
4.3	Settling Velocity and Flocculation .....	8
4.4	Sediment Concentration Profiles .....	10
4.4.1	Teeter 1986 profile .....	11
4.4.2	Rouse profile .....	11
4.5	Erosion .....	12
4.6	Bed Description .....	13
<b>5</b>	<b>Sand Transport.....</b>	<b>14</b>
5.1	Introduction.....	14
5.2	Near-bed and Suspended Load Sand Transport .....	14
5.2.1	Transport Tables .....	17
5.2.2	Suspended Load Transport.....	17
5.2.3	Near-bed Load Transport.....	17
5.2.4	Influence of Mud.....	18
5.2.5	Morphology.....	18
5.3	Fine Sand Sediment Transport .....	19
5.3.1	Suspended Load Transport.....	19
5.3.2	Settling Velocity.....	21
5.3.3	Sediment Concentration Profiles.....	22
5.3.4	Deposition .....	24
5.3.5	Erosion .....	24
<b>6</b>	<b>Hydrodynamic Variables.....</b>	<b>25</b>
6.1	Bed Shear Stress .....	25
6.1.1	Pure currents.....	25
6.1.2	Pure wave motion.....	25
6.1.3	Combined currents and waves.....	26
6.2	Viscosity and Density .....	28
6.2.1	Mud impact on density .....	28
6.2.2	Mud influence on viscosity .....	28

<b>7</b>	<b>Multi-Layer and Multi-Fraction Applications .....</b>	<b>30</b>
7.1	Introduction.....	30
7.2	Dense Consolidated Bed .....	30
7.3	Soft, Partly Consolidated Bed .....	31
<b>8</b>	<b>Morphological Features .....</b>	<b>32</b>
8.1	Morphological Simulations .....	32
8.2	Bed Update .....	32
<b>9</b>	<b>Sediment Disposal .....</b>	<b>34</b>
9.1	Nearfield model theory .....	34
9.1.1	Sediment Stripping .....	36
9.1.2	Sediment Fall-Out .....	37
9.1.3	Dynamic Bed Collapse Phase.....	38
9.2	Coupling of Nearfield model to MIKE FM.....	41
<b>10</b>	<b>Propeller wash.....</b>	<b>44</b>
10.1	Nearfield model theory .....	44
10.2	Bed shear stress caused by propeller induced jet flow over seabed .....	47
10.2.1	Simple log-law assumption .....	48
10.2.2	Advanced moving turbulent boundary layer assumption .....	48
10.3	Coupling of Nearfield model to MIKE FM.....	48
<b>11</b>	<b>References.....</b>	<b>49</b>

## 1 Introduction

The present Scientific Documentation aims at giving an in-depth description of the theory behind and equations used in the Mud Transport Module of the MIKE 21 & MIKE 3 Flow Model FM.

First a general description of the term "mud" is given. This is followed by a number of sections giving the physical, mathematical and numerical background for each of the terms in the cohesive sediment and fine sand transport equations.

Special sections describe the case of multi-layer and multi-fraction applications as well as the option of morphological simulations.

## 2 What is Mud

Mud is a term generally used for fine-grained and cohesive sediment with grain-sizes less than 63 microns. Mud is typically found in sheltered areas protected from strong wave and current activity. Examples are the upper and mid reaches of estuaries, lagoons and coastal bays. The sources of the fine-grained sediments may be both fluvial and marine.

Fine-grained suspended sediment plays an important role in the estuarine environment. Fine sediment is brought in suspension and transported by current and wave actions. In estuaries, the transport mechanisms (settling – and scour lag) acting on the fine-grained material tend to concentrate and deposit the fine-grained material in the inner sheltered parts of the area (Van Straaten & Kuenen, 1958; Postma, 1967; and Pejrup, 1988). A zone of high concentration suspension is called a turbidity maximum and will change its position within the estuary depending on the tidal cycle and the input of fresh-water from rivers, etc. (e.g. Dyer, 1986).

Fine sediments are characterised by low settling velocities. Therefore, the sediments may be transported over long distances by the water flow before settling. The cohesive properties of fine sediments allow them to stick together and form larger aggregates or flocs with settling velocities much higher than the individual particles within the floc (Krone, 1986; Burt, 1986). In this way they are able to deposit in areas where the individual fine particles would never settle. The formation and destruction of flocs are depending on the amount of sediment in suspension as well as the turbulence properties of the flow and the salinity. This is in contrast to non-cohesive sediment, where the particles are transported as single grains.



Figure 2-1 Muddy (left) and sandy (right) sediments

Fine sediment is classified according to grain-size as shown in Table 2.1.

Table 2.1 Classification of fine sediment

Sediment type	Grain size	Flocculation ability
Clay	< 4 $\mu\text{m}$	high
Silt	4-63 $\mu\text{m}$	medium
Fine sand	63-125 $\mu\text{m}$	very low/no flocculation

### 3 General Model Description

#### 3.1 Introduction

In order to include the transport and deposition processes of fine-grained material in the modelling system, it is necessary to integrate the description with the advection-diffusion equation caused by the water flow.

The transport and deposition processes of fine-grained material is included in the modelling system by integrating the sediment transport processes with the flow-generated advection and diffusion.

MIKE 21 & MIKE 3 Flow Model FM is based on a flexible mesh approach and has been developed for applications within oceanographic, coastal and estuarine environments. In the case of 2D, the model is depth-integrated. This means that the simulation of the transport of fine-grained material must be averaged over depth and appropriate parameterisations of the sediment processes must be applied.

In the MIKE 21 & MIKE 3 Flow Model FM model complex, the transport of fine-grained material (mud) has been included in the Mud Transport module (MT), linked to the Hydrodynamic module (HD), as indicated in Figure 3-1.

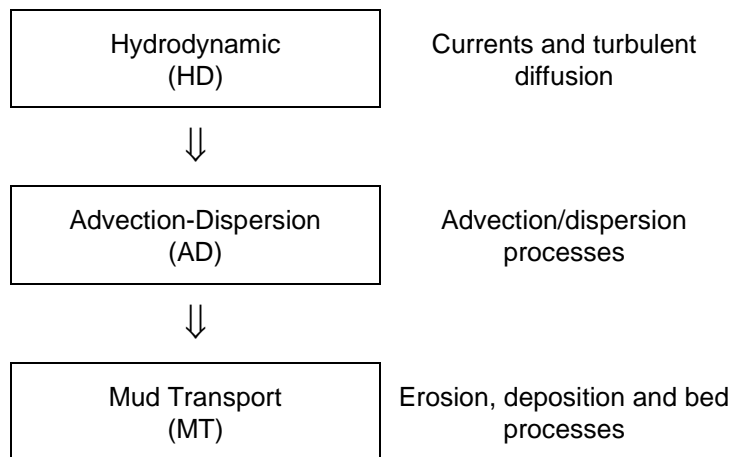


Figure 3-1 Data flow and physical processes for MIKE 21 & MIKE 3 Flow Model FM, Mud Transport calculation

The processes included in the Mud Transport module are kept as general as possible. The Mud Transport module includes the following processes:

- Multiple mud fractions
- Multiple bed layers
- Wave-current interaction
- Flocculation
- Hindered settling
- Inclusion of a sand fraction
- Transition of sediments between layers
- Simple morphological calculations

The above possibilities cover most cases appropriate for 2D modelling. In case special applications are required such as simulating the influence of high sediment concentrations on the water flow through formation of stratification and damping of turbulence, the modeller is referred to 3D modelling.

## 3.2 Governing Equations 2D

The sediment transport formulations are based on the depth-integrated advection-dispersion calculations in the Hydrodynamic module.

The Mud Transport module solves the so-called advection-dispersion equation:

$$\frac{\partial \bar{c}}{\partial t} + u \frac{\partial \bar{c}}{\partial x} + v \frac{\partial \bar{c}}{\partial y} = \frac{1}{h} \frac{\partial}{\partial x} \left( h D_x \frac{\partial \bar{c}}{\partial x} \right) + \frac{1}{h} \frac{\partial}{\partial y} \left( h D_y \frac{\partial \bar{c}}{\partial y} \right) + Q_L C_L \frac{1}{h} - S \quad (3.1)$$

where

$\bar{c}$	depth averaged concentration (kg/m <sup>3</sup> )
$u, v$	depth averaged flow velocities (m/s)
$x, y$	horizontal coordinates
$D_x, D_y$	dispersion coefficients (m <sup>2</sup> /s)
$h$	water depth (m)
$S$	deposition/erosion term (g/m <sup>3</sup> /s)
$Q_L$	source discharge per unit horizontal area (m <sup>3</sup> /s/m <sup>2</sup> )
$C_L$	concentration of the source discharge (g/m <sup>3</sup> )

In cases of multiple sediment fractions, the equation is extended to include several fractions while the deposition and erosion processes are connected to the number of fractions. It is noted that the fall velocity enters the equation in the expression for the deposition, see Section 4.2.

## 3.3 Numerical Schemes

The advection-dispersion equation is solved using an explicit, third-order finite difference scheme, known as the ULTIMATE scheme (Leonard, 1991). This scheme is based on the well-known QUICKEST scheme (Leonard, 1979; Ekebjærg & Justesen, 1991).

This scheme has been described in various papers dealing with turbulence modelling, environmental modelling and other problems involving the advection-dispersion equation. It has several advantages over other schemes, especially that it avoids the "wiggle" instability problem associated with central differentiation of the advection terms. At the same time it greatly reduces the numerical damping, which is characteristic of first-order up-winding methods.

The scheme itself is a Lax-Wendroff or Leith-like scheme in the sense that it cancels out the truncation error terms due to time differentiation up to a certain order by using the basic equation itself. In the case of QUICKEST, truncation error terms up to third-order are cancelled for both space and time derivatives.

The solution of the erosion and the deposition equations are straightforward and do not require special numerical methods.

## 4 Cohesive Sediments

### 4.1 Introduction

The Mud Transport module of MIKE 21 & MIKE 3 Flow Model FM describes the erosion, transport and deposition of fine-grained material  $< 63 \mu\text{m}$  (silt and clay) under the action of currents and waves. For a correct solution of the erosion processes, the consolidation of sediment deposited on the bed is also included. The model is essentially based on the principles in Mehta et al. (1989) with the innovation of including the bed shear stresses due to waves.

Clay particles have a plate-like structure and an overall negative ionic charge due to broken mineral bonds on their faces. In saline water, the negative charges on the particles attract positively charged cations and a diffuse cloud of cations is formed around the particles. In this way the particles tend to repel each other (Van Olphen, 1963). Still, particles in saline water flocculate and form large aggregates or flocs in spite of the repulsive forces. This is because in saline water, the electrical double layer is compressed and the attractive van der Waals force acting upon the atom pairs in the particles becomes active. Flocculation is governed by increasing concentration, because more particles in the water enhance meetings between individual particles. Turbulence also plays an important role for flocculation both for the forming and breaking up of flocs depending on the turbulent shear (Dyer, 1986).

A deterministic physically based description of the behaviour of cohesive sediment has not yet been developed, because the numerous forces included in their behaviour tend to complicate matters. Consequently, the mathematical descriptions of erosion and deposition are essentially empirical, although they are based on sound physical principles.

The lack of a universally applicable, physically based formulation for cohesive sediment behaviour means that any model of this phenomenon is heavily dependent on field data (Andersen & Pejrup, 2001; Andersen, 2001; Edelvang & Austen, 1997; Pejrup et al., 1997). Extensive data over the entire area to be modelled is required such as:

- bed sedimentology
- bed erodibility
- biology
- settling velocities
- suspended sediment concentrations
- current velocities
- vertical velocity and suspended sediment concentration profiles
- compaction of bed layers
- effect of wave action
- critical shear stresses for deposition and erosion

Of course, the dynamic variation of water depth and flow velocities must also be known along with boundary values of suspended sediment concentration.

The Mud Transport module consists of a 'water-column' and an 'in-the-bed' module. The link between these two modules is source/sink terms in an advection-dispersion model.

The transport and deposition of fine-grained material is governed by the fact that settling velocities are generally slow compared to sand. Hence, the concentration of suspended material does not adjust immediately to changes in the hydraulic conditions. In other words, the sediment concentration at a given time and location is dependent on the

conditions upstream of this location at an earlier time. Postma (1967) first described this process, called settling- and scour-lag. This is the main factor for the concentration of fine material in estuaries often resulting in a turbidity maximum. In order to describe this process, the sediment computation has been built into the advection-dispersion formulation in the Hydrodynamic module.

For 3D calculations the viscosity and density may be influenced by large concentrations of mud in the water column.

The source and sink term  $S$  in the advection-dispersion equation depends on whether the local hydrodynamic conditions cause the bed to become eroded or allow deposition to occur. Empirical relations are used, and possible formulations for evaluating  $S$  are given below.

The mobile suspended sediment is transported by long-period waves only, which are tidal currents, whereas the wind-waves are considered as "shakers". Combined they are able to re-entrain or re-suspend the deposited or consolidated sediment.

The processes in the bed are described in a multi-layer bed; each layer is described by a critical shear stress for erosion, erosion coefficient, power of erosion, density of dry sediment and erosion function.

The bed layers can be soft and partly consolidated or dense and consolidated.

Consolidation is included as a transition rate of sediment between the layers and liquefaction by waves is included as a weakening of the bed due to breakdown of the bed structure.

A conceptual illustration of the physical processes modelled by a "multi bed layer approach" is shown in Figure 4-1.

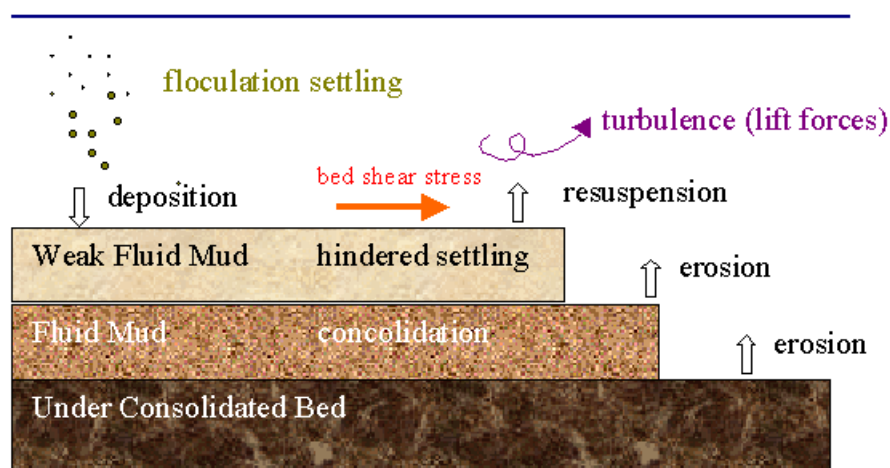


Figure 4-1 Multi-layer model and physical processes for example with three bed layers

## 4.2 Deposition

In the MT model, a stochastic model for flow and sediment interaction is applied. This approach was first developed by Krone (1962).

Krone suggests that the deposition rate can be expressed by:

$$\text{Deposition : } S_D = w_s c_b p_d \quad (4.1)$$

where

$w_s$	settling velocity (m/s)
$c_b$	near bed concentration (kg/m <sup>3</sup> )
$p_d$	probability of deposition

The probability of deposition  $p_d$  is calculated as:

$$p_d = 1 - \frac{\tau_b}{\tau_{cd}} = \tau_b \leq \tau_{cd} \quad (4.2)$$

where

$\tau_b$	the bed shear stress (N/m <sup>2</sup> )
$\tau_{cd}$	the critical bed shear stress for deposition (N/m <sup>2</sup> )

### 4.3 Settling Velocity and Flocculation

The settling velocity of the fine sediment depends on the particle/floc size, temperature, concentration of suspended matter and content of organic material.

Usually one distinguishes between a regime where the settling velocity increases with increasing concentration (flocculation) and a regime where the settling velocity decreases with increasing concentration. The latter is referred too as hindered settling. The first is the most common of the two in the estuary.

Following Burt (1986), the settling velocity in saline water (>5 ppt) can be expressed by:

$$w_s = kc^\gamma \text{ for } c \leq 10 \text{ kg/m}^3 \quad (4.3)$$

where

$w_s$	settling velocity of flocs (m/s)
$c$	volume concentration
$k, \gamma$	coefficients
$\gamma$	1 to 2

The relation for  $c \leq 10 \text{ kg/m}^3$  describes the flocculation of particles based on particle collisions. The higher concentration the higher possibility for the particles to flocculate.

$c > 10 \text{ kg/m}^3$  corresponds to 'hindered' settling, where particles are in contact with each other and do not fall freely through the water.

Alternative settling formulations are also available:

The formulation of Richardson and Zaki (1954) is the classical equation for hindered settling:

$$w_s = w_{s,r} \left( 1 - \frac{c}{c_{gel}} \right)^{w_{s,n}} \quad (4.4)$$

Where  $w_{s,r}$  is a reference value,  $w_{s,n}$  a coefficient and  $c_{gel}$  the concentration at which the flocs start to form a real self-supported matrix (referred to as the gel point).

Winterwerp (1999) proposed the following for hindered settling:

$$w_s = w_{s,r} \frac{(1 - \Phi_*) (1 - \Phi_p)}{1 + 2.5\Phi} \tag{4.5}$$

where

$$\Phi_p = \frac{c}{\rho_s} \tag{4.6}$$

and  $\rho_s$  is the density of sediment grains.

Flocculation is enhanced by high organic matter content including organic coatings, etc. (Van Leussen, 1988; Eisma, 1993). In fresh water, flocculation is dependent on organic matter content, whereas in saline waters salt flocculation also occurs. The influence of salt on flocculation is primarily important in areas where fresh water meets salt water such as estuaries. The following expression is used to express the variation of settling velocity with salinity. Please note that the reference value  $w_s$  is the value representative for saline water:

$$w_s = w_s (1 - C_1 e^{C_2}) \tag{4.7}$$

where  $C_1$  and  $C_2$  are calibration parameters.

Figure 4-2 shows an example of  $C_1 = \{0, 0.5, 1\}$  and  $C_2 = -1/3$ .

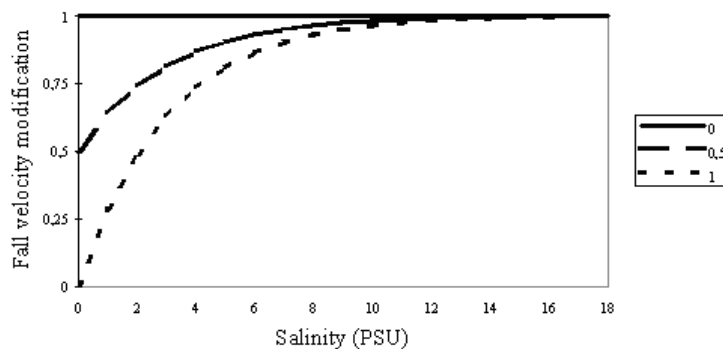


Figure 4-2 Settling velocity and salinity dependency

The description of salt flocculation is based on Krone's experimental research (Krone, 1962) Whitehouse et al., (1960) studied the effect of varying salinities on flocculation of different clay minerals in the laboratory. Gibbs (1985) showed that in the natural environment, flocculation is more dependent on organic coating. Therefore, the effect of mineral constitution of the sediment is not taken into account in the model.

### 4.4 Sediment Concentration Profiles

Two expressions for the sediment concentration profile can be applied. Either an expression that is based on an approximate solution to the vertical sediment fluxes during deposition (Teeter) or an expression that assumes equilibrium between upward and downward sediment fluxes (Rouse).

The difference between the two expressions is depicted in Figure 4-3.

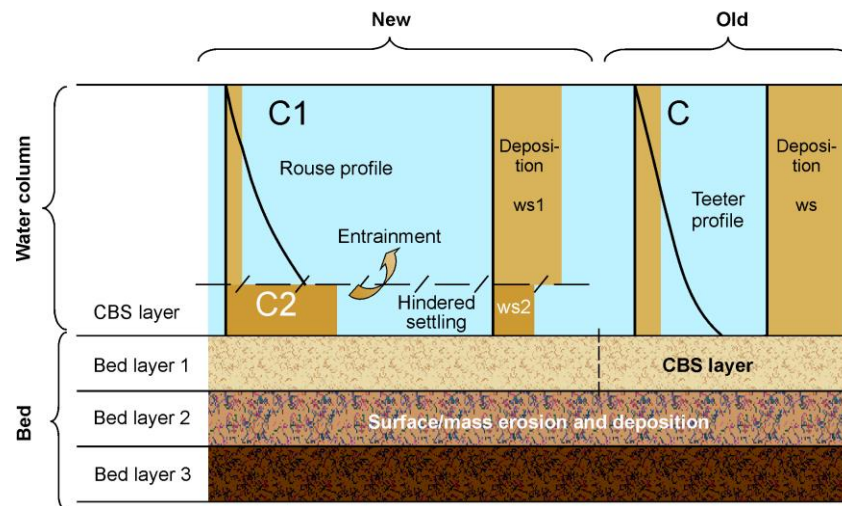


Figure 4-3 Definition of Rouse profile vs. Teeter profile

The near bed concentration  $c_b$  is proportional to the depth averaged mass concentration  $\bar{c}$  and is related to the vertical transport, i.e. a ratio of the vertical convective and diffusive transport represented by the Peclet number  $P_e$ :

$$P_e = \frac{C_{rc}}{C_{rd}} \tag{4.8}$$

where

$C_{rc}$  convective Courant number =  $w_s \Delta t / h$

$C_{rd}$  diffusive Courant number =  $\bar{D}_z \Delta t / h^2$

$w_s$  mean settling velocity of the sediment

$\bar{D}_z$  depth mean eddy diffusivity

#### 4.4.1 Teeter 1986 profile

In this expression the near bed concentration  $c_b$  is related to the depth averaged concentration  $\bar{c}$  (Teeter, 1986):

$$\beta = \frac{c_b}{\bar{c}} \quad (4.9)$$

where

$$\beta = 1 + \frac{P_e}{1.25 + 4.75 p_d^{2.5}} \quad (4.10)$$

$$P_e = \frac{w_s h}{D_z} = \frac{6w_s}{\kappa U_f} \quad (4.11)$$

$\kappa$  Von Karman's universal constant ( $\kappa = 0.4$ )

$U_f$  Friction velocity  $\sqrt{\tau_b / \rho}$

#### 4.4.2 Rouse profile

The suspended sediment is affected by turbulent diffusion, which results in an upward motion. This is balanced by settling of the grains. The balance between diffusion and settling can be expressed:

$$-\varepsilon \frac{dC}{dz} = w_s C \quad (4.12)$$

where

$\varepsilon$  diffusion coefficient

$C$  concentration as function of  $z$

$z$  vertical Cartesian coordinate

By assuming that  $\varepsilon$  is equal to the turbulent eddy viscosity, and applying the parabolic eddy viscosity distribution

$$\varepsilon = \kappa U_f z \left( 1 - \frac{z}{h} \right) \quad (4.13)$$

where

$h$  height of water column

the following vertical concentration profile will be given:

$$C = C_a \left[ \frac{a}{h-a} \frac{h-z}{z} \right]^R, a \leq z \leq h \quad (4.14)$$

where

$C_a$  reference concentration at  $z = a$   
 $a$  reference level  
 $R$  Rouse number

$$R = \frac{w_s}{\kappa U_f} \quad (4.15)$$

It is possible to choose a vertical variation of the concentration of suspended sediment in order to determine the settling distance. The average depth,  $h^*$  through which the particles settle at deposition is given by:

$$\frac{h^*}{h} = \frac{\int_0^1 s \left( \frac{1-s}{s} \right)^R ds}{\int_0^1 \left( \frac{1-s}{s} \right)^R ds} \quad (4.16)$$

where  $s = h/z$  and the term  $\frac{h^*}{h}$  is named the relative height of centroid.

The near bed suspended sediment concentration  $c_b$  is related to the depth-averaged concentration  $\bar{c}$  using the Rouse profile

$$c_b = \frac{\bar{c}}{RC} \quad (4.17)$$

in which  $RC$  is the relative height of centroid.

## 4.5 Erosion

Erosion can be described in two ways depending upon whether the bed is dense and consolidated (Partheniades, 1965) or soft and partly consolidated (Parchure and Mehta, 1985).

For dense, consolidated bed the erosion ( $S_E$ ) is defined by:

$$S_E = E \left( \frac{\tau_b}{\tau_{ce}} - 1 \right)^n, \tau_b > \tau_{ce} \quad (4.18)$$

where

$E$  erodibility of bed ( $\text{kg/m}^2/\text{s}$ )  
 $\tau_b$  bed shear stress ( $\text{N/m}^2$ )

$\tau_{ce}$  critical bed shear stress for erosion (N/m<sup>2</sup>)

$n$  power of erosion

For soft, partly consolidated bed the erosion is defined by:

$$S_E = E \exp\left[\alpha(\tau_b - \tau_{ce})^{1/2}\right], \tau_b > \tau_{ce} \quad (4.19)$$

where

$\alpha$  coefficient ( $m/\sqrt{N}$ )

## 4.6 Bed Description

It is possible to describe the bed as having more than one layer. Each layer is described by the critical shear stress for erosion,  $\tau_{ce,j}$ , power of erosion,  $n_j$ , density of dry bed material,  $\rho_i$ , erosion coefficient,  $E_j$ , and  $\alpha_j$ -coefficient. The deposited sediment is first included in the top layer. The layers represent weak fluid mud, fluid mud and under-consolidated bed (Mehta et al., 1989) and are associated with different time scales.

The model requires an initial thickness of each layer to be defined.

The consolidation process is described as the transition of sediment between the layers (Teisson, 1992; Sanford and Maa, 2001).

The influence of waves is taken into account as liquefaction resulting in a weakening of the bed due to breakdown of bed structure. This may cause increased surface erosion, because of the reduced strength of the bed top layer (Delo and Ockenden, 1992).

## 5 Sand Transport

### 5.1 Introduction

In many estuaries the sediment is composed of a mixture of sand and mud or sand in some places (usually in the tidal channels) and mud in other places (on the mud flats), therefore it is advantageous to be able to model both sand and mud in the same model.

This presents a number of difficult challenges because the interaction of sand and mud is rather poorly understood, mainly due to lack of data (see van Rijn 2020). Therefore, the different sand and mud fractions are often treated separately in numerical models, and the interaction of the two fractions is ignored. This is also the approach taken in the MT module.

The major differences between a cohesive dominated sediment bed and a non-cohesive dominated sediment bed are the initiation of motion of sediment particles and the absence of bed load sediment transport in the cohesive case.

In case the sediment bed is dominated by cohesive sediment, the sand in the bed is engrained in the bed and erodes in a similar manner as the cohesive sediment in the bed, as flakes which are teared from the bed. In this case there will be no bed load transport of sand along the bed as the flakes are brought directly into suspension. This situation can be modelled using the “Fine Sand Sediment Transport” model.

In case the bed is dominated by non-cohesive sediment, the sand will be transported along the bed as bed load, in this case the “General Sand Transport” model should be used. In general, we recommend using this model unless only suspended load transport is important for the problem being modelled. An example where only suspended load transport is important is sand spilled during dredging operations in areas where the sand is never mobilised after it deposits on the seabed.

The two models are described in the following subsections.

### 5.2 Near-bed and Suspended Load Sand Transport

The “near-bed and suspended load sand transport” model uses DHI’s Sand Transport Program (STP) to calculate the transport of sand for combined waves and currents. This is achieved through the application of sand transport tables similar to what is done in the MIKE 21/3 FM Sand Transport module for combined waves and currents. Here, the sediment transport rates are defined as function of a number of typical wave- and current parameters and the granulometric characteristics of the sand.

The model separates the sand transport into two parts:

- Near-bed load transport
- Suspended load transport

The near-bed load transport is the transport of sand on and within a short distance  $z_{wb}$  from the bed. It is the sum of the traditional bed load transport (grains rolling along the bed) and suspended load transport occurring within the distance  $z_{wb}$  from the bed. The near-bed load transport responds quickly to changes in the hydrodynamic forcing because the transport occurs close to the bed and the near-bed load transport is therefore assumed to always be in equilibrium with the local forcing conditions.

The suspended load transport is the transport occurring at a distance larger than  $z_{wb}$  from the bed (see Figure 5-1). This transport is calculated using the advection-diffusion solver in a similar manner to how the mud transport is calculated in the MT model.

The distance  $z_{wb}$  is determined in STP. STP calculates the transport due to combined waves and current. The hydrodynamic description is based on the turbulent boundary layer due to combined wave- current motion as presented in Fredsøe (1984). The vertical distribution of the time averaged shear stress is calculated according to Deigaard and Fredsøe (1989). Turbulence originating from breaking waves is calculated according to Deigaard et al (1986). The suspended sediment transport is calculated using the model of Fredsøe et al (1985). The vertical variation of the instantaneous sediment flux,  $q(t,z)$  is calculated as :

$$q(t,z) = u(t,z) * c(t,z) \quad (5.1)$$

Where  $u(t,z)$  is flow velocity,  $c$  = suspended sediment concentration,  $t$ = time and  $z$  = height above the bed.

Time averaged values of  $u$ ,  $c$  and  $q$  are obtained by averaging over one wave period.

Close to the bed, the flow is dominated by the wave motion. Here the sediment concentration and the transport vary strongly with the instantaneous bed shear stress. However, further away from the bed, the shear / turbulence due to the mean flow starts to dominate and the concentration varies less and less.

The sediment concentration does not vary linearly with the flow velocity. Therefore,

$$\overline{q(t)} = \overline{u(z)c(z)} \neq \overline{u(z)} \overline{c(z)} \quad (5.2)$$

However, the difference between  $\overline{uc}$  and  $\overline{u} \overline{c}$  decreases with distance above the bed. The level  $z_{wb}$  is defined as the elevation above the bed where this difference becomes < 5%.

Figure 5-1 shows an example of the mean velocity, concentration and transports over the water depth calculated by STP.

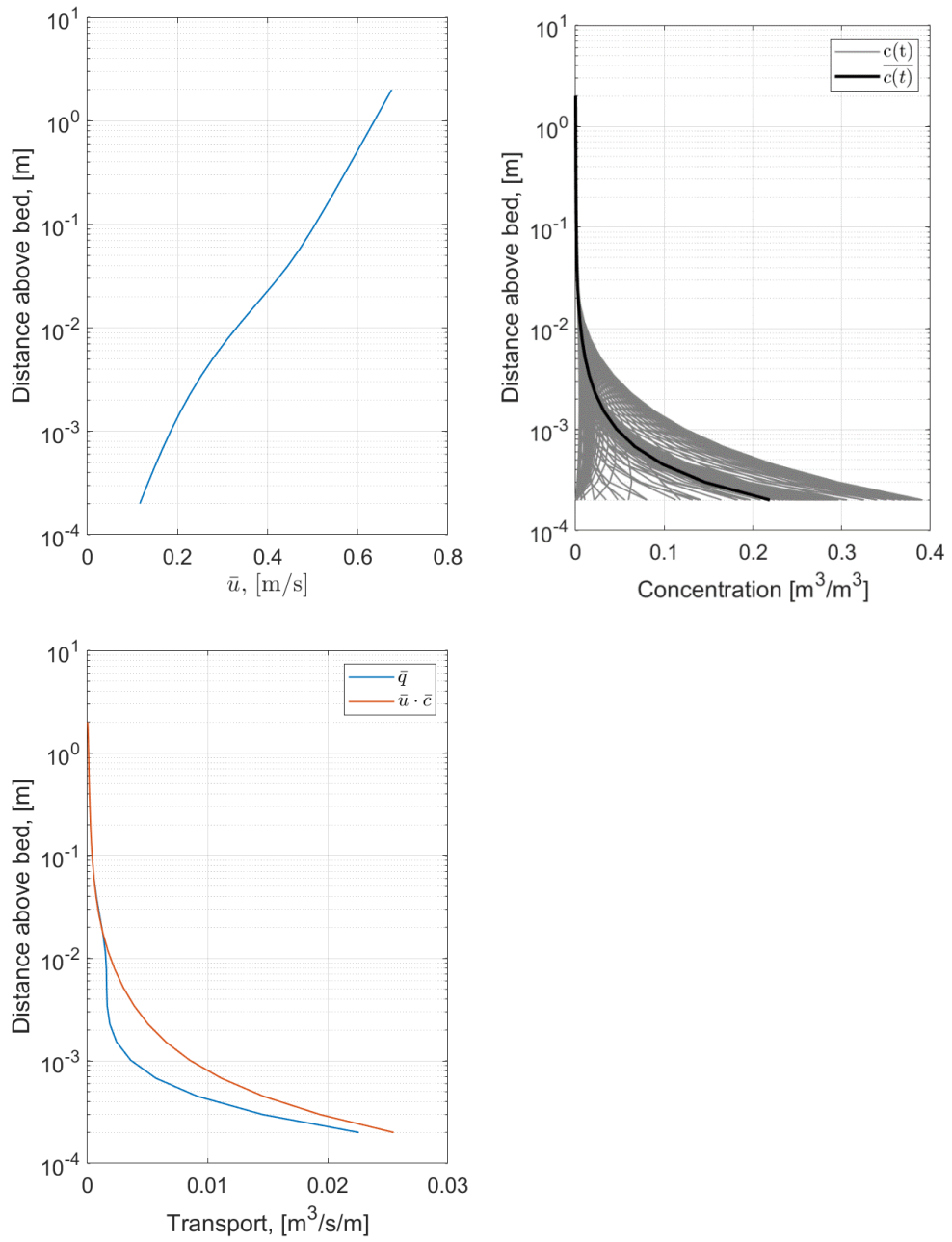


Figure 5-1: Top left: Mean velocity. Top right: Concentration during wave period,  $c(t)$ , and mean concentration,  $\bar{c}(t)$ . Bottom left: Mean transport and mean velocity times mean concentration. In this example  $z_{wb}$  is around  $10^{-2}$  m.

## 5.2.1 Transport Tables

In the *near-bed and suspended load transport model* 6 tables generated using the are needed. These tables are

- Near-bed load sand transport in the direction of the mean bed shear stress (Table.lon) and
- Near-bed load sand transport perpendicular to this direction (Table.crs)
- Distance from the bed separating the near-bed load and suspended load transport,  $z_{wb}$  (Table.cen)
- Concentration at  $z_{wb}$  from the bed (Table.con)
- Current friction velocity,  $u_{fc}$  (Table.ufc)
- Wave induced roughness height,  $k_{nw}$  (Table.knw)

All these tables are needed for the model to run.

The tables are generated with STP, please see the scientific documentation for MIKE 21/3 FM Sand Transport Module for a detailed description of the STP model.

## 5.2.2 Suspended Load Transport

The suspended load transport in the MT module is handled by solving the advection-diffusion equation for the suspended sediment subject to bottom and surface boundary conditions.

At the surface the boundary condition is zero influx of sediment from the surface. At the bed, the boundary condition is given by specifying the concentration in the bottom cell by interpolation in the concentration table generated from STP.

However, the table contains the concentration at distance  $z_{wb}$  from the bed, a Vanoni profile (equation 4.14) is used to transform the concentration at  $z_{wb}$ , to the concentration in the center of the bottom cell.

## 5.2.3 Near-bed Load Transport

The transport table (Table.lon) contains the transport integrated up to the distance  $z_{wb}$  above the bed, i.e.  $q_{wb}$ . To this, we add the transport integrated up to the center of the bottom cell ( $z_{cell}$ ) by adding the integral of the Vanoni profile (equation 4.14) multiplied with a log-velocity profile

$$\frac{\overline{u(z)}}{U_{fc}} = \frac{1}{\kappa} \log \left( \frac{z}{k_{nw}/30} \right) \quad (5.3)$$

where  $\overline{u(z)}$  is the mean current speed at level  $z$ ,  $U_{fc}$  is the current friction velocity,  $k_{nw}$  is the wave induced bed roughness height and  $\kappa$  is von Karmans constant.  $U_{fc}$  and  $k_{nw}$  are interpolated from the tables generated by STP.

Thus

$$q_{nearbed} = q_{wb} + \int_{z_{wb}}^{z_{cell}} \overline{u(z)} \times \overline{c(z)} dz - z_{cell} \times \overline{c(z_{cell})} \times \overline{u(z_{cell})} \quad (5.4)$$

The last term compensates for the transport from the bed to the center of the bottom cell included in the advection-diffusion solver.

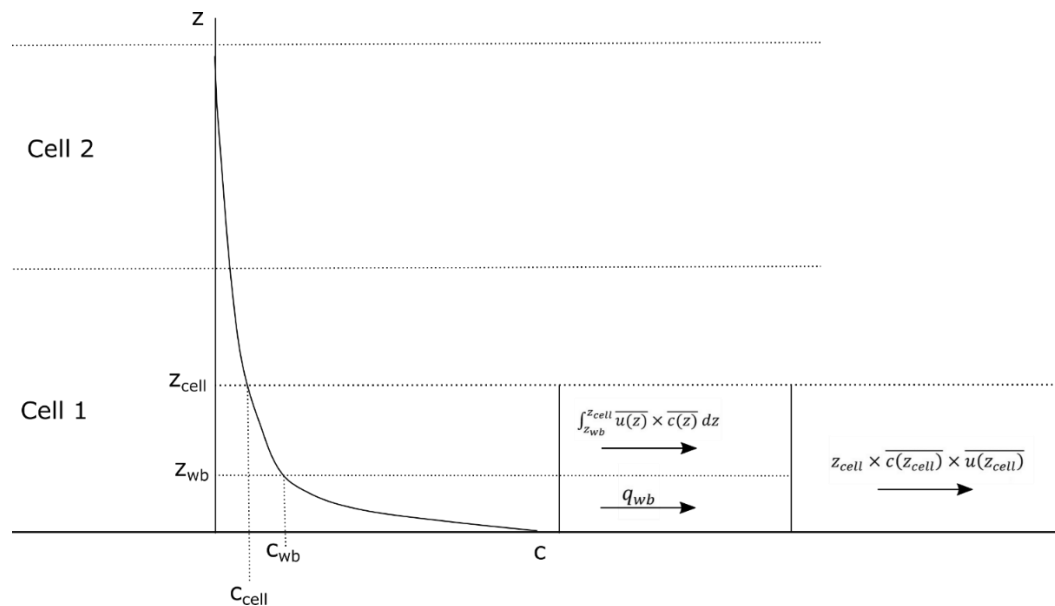


Figure 5-2: Sketch of  $z_{wb}$ ,  $c_{wb}$  and  $z_{cell}$ .

### 5.2.4 Influence of Mud

Both the near-bed transport rates and the bed concentration interpolated from the sediment tables are reduced according to the mass-percentage of sand in the active layer of the bed at each computational element in the model. Thus, in case the mass-percentage of sand in active layer in the bed is 40 %, then the near-bed transport rates and the near bed concentration are multiplied by a factor of 0.4.

### 5.2.5 Morphology

In the *near-bed and suspended load transport model* there are two contributions to the erosion and deposition:

- Spatial gradients in the near-bed load transport .
- Changes in the suspended concentration in the bottom cell

Spatial gradients in the near-bed transport lead to changes in the mass of the cell. Bed level changes are calculated in a similar manner as changes due to gradients in bed load in the MIKE 21 FM Sand Transport module. The calculation is the same, except that the resulting bed level change is converted to a change in bed mass (of the sand fraction).

$$\frac{dz}{dt} = \frac{1}{n-1} * \frac{dq}{dx} \tag{5.5}$$

Deposition due to changes in the suspended concentration in the bottom cell is calculated as:

$$S_d = -(c_{cell} - c) * w_s^*, \quad c_{cell} < c \tag{5.6}$$

Where  $w_s^*$  is the scaled fall velocity given by:

$$w_s^* = \frac{0.5 w_s}{ft} \quad (5.7)$$

Where  $ft = \frac{h^*}{h}$ , given by equation 4.16, is the relative height of the centroid of the concentration profile. For non-uniform profiles  $ft$  is smaller than 0.5 resulting in an increase in the scaled fall velocity. In the *near-bed and suspended load transport* model  $ft = 0.5$  because the non-uniform profile has been accounted for in the near-bed load transport.

Similarly, erosion is calculated as:

$$S_e = -(c_{cell} - c) * w_s^*, \quad c_{cell} > c \quad (5.8)$$

## 5.3 Fine Sand Sediment Transport

The *near-bed and suspended load transport* model is quite demanding computationally, this is because the interpolation in the transport tables needs to happen at every AD time step in the model. In case waves are not important and the sand transport is dominated by suspended load transport in a cohesive bed environment, a simpler sand transport model can be used. This is the “Fine Sand Sediment Transport” model described in the present sub-section. Note that this model is named “Suspended load” when selecting on the GUI and in the on-line help.

### 5.3.1 Suspended Load Transport

The equilibrium concentration  $\bar{c}_e$  is defined as:

$$\bar{c}_e = \frac{q_s}{\bar{u}h} \quad (5.9)$$

Where

$\bar{u}$  is the depth averaged flow velocity

$q_s$  suspended load transport (kg/m/s)

The suspended load transport is found as the integral of the current velocity profile,  $u$ , and the concentration profile of suspended sediment,  $c$ :

$$q_s = \int_a^h u \cdot c \cdot dy \quad (5.10)$$

where

$c$  concentration of sediment (kg/m<sup>3</sup>) at distance  $y$  from bed

$u$  flow velocity (m/s) at distance  $y$  from bed

$h$  water depth (m)

$a$  thickness of the bed layer (m)

Usually little is known about the bed layer, such as the height of the bed forms. This results in the approximation:

$$a = k_s = 2d_{50} \quad (5.11)$$

Where:

$k_s$  equivalent roughness height (m)  
 $d_{50}$  50 percent fractile of grain-size of sediment (m)

In the advection-dispersion model, the suspended transport is calculated based on depth-averaged flow velocities,  $\bar{u}, \bar{v}$ , a compound concentration,  $\bar{c}$ , and the water depth,  $h$ , (approx.  $h \approx h - a$ ). The sand transport is described through a depth-averaged equilibrium concentration,  $\bar{c}_e$  and an accretion (deposition), erosion term,  $S$ . This formulation means that no bed transport takes place.

The transport is highly dependent upon two parameters, namely the settling velocity,  $w_s$ , and the turbulent sediment diffusion coefficient,  $\varepsilon_s$ , because these parameters have an effect on both the flow velocity and concentration profile. For a normal sediment load the effect on the velocity profile is negligible.

### Requirements for sediments in suspension

The following description is mainly based on Van Rijn (1982, 1984), Yalin (1972) and Engelund and Fredsøe (1976).

For sediments to stay in suspension it is required that the actual friction velocity,  $U_f$ , is larger than a so-called critical friction velocity,  $U_{f,cr}$ , and that the vertical turbulence is sufficient to create vertical velocity components higher than the settling velocity.

The first assumption is expressed through the transport stage parameter,  $T$ :

$$T = \begin{cases} \left( \frac{U_f}{U_{f,cr}} \right)^2 - 1, & U_f > U_{f,cr} \\ 0, & U_f \leq U_{f,cr} \end{cases} \quad (5.12)$$

where  $U_{f,cr}$  is found from Shields curve, see Rijn (1982), using the input parameters,  $d_{50}$ , relative density of sediment,  $s$ , and the dimensionless grain size,  $d^*$ , defined as the cube root of the ratio of immersed weight to viscous forces:

$$d^* = d_{50} \left[ \frac{(s-1)g}{\nu^2} \right]^{1/3} \quad (5.13)$$

where  $\nu$  is the kinematic viscosity of water ( $m^2/s$ ).

The friction velocity,  $U_f$ , reads:

$$U_f = \frac{\sqrt{g}}{C_z} |\vec{V}| \quad (5.14)$$

Where:

$I$	energy gradient (slope)
$C_z$	Chezy Number ( $m^{1/2}/s$ ) ( $= 18 \ln(4h/d_{90})$ )
$d_{90}$	90 percent fractile of grain size of sediment (m)
$ \vec{V} $	flow speed (m/s)

The second assumption is expressed through some relations between the critical friction velocity,  $U_{f,crs}$  for initiation of suspension, the settling velocity,  $w_s$  and  $d^*$ :

$$\frac{U_{f,crs}}{w_s} = \begin{cases} \frac{4}{d^*}, & 1 < d^* \leq 10 \\ 0.4 & d^* > 10 \end{cases} \quad (5.15)$$

### 5.3.2 Settling Velocity

The settling velocity for fine sand depends on the particle size, kinematic viscosity and sediment density.

The settling velocity is expressed by:

$$w_s = \begin{cases} \frac{(s-1)gd^2}{18\nu}, & d < 100\mu m \\ \frac{10\nu}{d} \left\{ \left[ 1 + \frac{0.01(s-1)gd^3}{\nu^2} \right]^{0.5} - 1 \right\}, & 100 < d \leq 1000\mu m \\ 1.1[(s-1)gd]^{0.5}, & d > 1000\mu m \end{cases} \quad (5.16)$$

Where:

$d$	grain size
$s$	sediment density
$\nu$	kinematic viscosity
$g$	acceleration due to gravity

### 5.3.3 Sediment Concentration Profiles

The concentration profile is dependent upon the turbulent sediment diffusion coefficient,  $\varepsilon_s$ , and the settling velocity,  $w_s$ . When calculating mud transport  $\varepsilon_s = \varepsilon_f$  is assumed, where  $\varepsilon_f$  is the turbulent flow diffusion coefficient, whereas for fine sand transport the assumption is:

$$\varepsilon_s = \beta \Phi \varepsilon_f \quad (5.17)$$

Where:

- $\beta$  factor, which describes the difference in the diffusion of a discrete sediment particle and the diffusion of a fluid "particle".
- $\Phi$  factor, which expresses the damping of the fluid turbulence by the sediment particles. Dependent upon local sediment concentration.

#### Diffusion factor

The interpretation of  $\beta$  is not quite clear. Some authors think that  $\beta < 1$ , because particles cannot respond fully to turbulent velocity fluctuations. However, others think that  $\beta > 1$ , because in the turbulent flow the centrifugal forces on the sediment particles would be greater than those on the fluid particles, thereby causing the sediment particles to be thrown to the outside of the eddies with a consequent increase in the effective mixing length and diffusion rate. In this model the following is used:

$$\beta = \begin{cases} 1 + \left( \frac{w_s}{U_f} \right)^2 & , \quad \frac{w_s}{U_f} < 0.5 \\ 1 & , \quad 0.5 \leq \frac{w_s}{U_f} < 2.5 \\ \text{no suspension} & , \quad \frac{w_s}{U_f} \geq 2.5 \end{cases} \quad (5.18)$$

#### Damping factor

The  $\Phi$  factor expresses the influence of the sediment particles on turbulence structure (damping effects) of the fluids.

In order to describe the concentration profile the following equation shall be solved:

$$\frac{dc}{dz} = \frac{w_s c(1-c)^5}{\varepsilon_s} \quad (5.19)$$

The determination of  $\Phi$  and the solution of this equation are very time-consuming, which leads to a more simplified method, which is chosen in this model.

#### Concentration profiles

The distribution of the concentration profile is described by the Peclet number,  $P_e$ :

$$P_e = \frac{C_{rc}}{C_{rd}} \quad (5.20)$$

Where:

- $C_{rc}$  convective Courant number ( $= w_s \Delta t/h$ )  
 $C_{rd}$  diffusive Courant number ( $= \varepsilon_f \Delta t/h^2$ )  
 $\varepsilon_f$  depth averaged fluid diffusion coefficient

This Peclet number is also called a suspension parameter,  $Z$ :

$$Z = \frac{w_s}{\beta \kappa U_f} \quad (5.21)$$

Where:

- $Z$  suspension parameter  
 $\kappa$  Von Karman's universal constant ( $\kappa = 0.4$ )  
 $\beta$  factor (as described in Eq. (5.18) above)

To take into account effects other than those caused by the  $\beta$  factor, a modified suspension parameter,  $Z'$  is defined as:

$$Z' = Z + \varphi \quad (5.22)$$

where  $\varphi$  is an overall correction factor, which reads:

$$\varphi = 2.5 \left( \frac{w_s}{U_f} \right)^{0.8} \left( \frac{c_a}{c_0} \right)^{0.4} \quad (5.23)$$

Where:

- $c_a$  concentration at reference level,  $z = a$   
 $c_0$  concentration at bed,  $z = 0$

The  $c_a/c_0$  concentration ratio is found through the following profiles:

$$\frac{C}{C_a} = \begin{cases} \frac{c}{c_a} = \left[ \frac{a(h-z)}{z(h-a)} \right]^Z, & \frac{z}{h} < 0.5 \\ \frac{c}{c_a} = \left[ \frac{a}{h-a} \right]^Z \exp\left(-4Z\left(\frac{z}{h} - 0.5\right)\right), & \frac{z}{h} \geq 0.5 \end{cases} \quad (5.24)$$

$c_a$  is based on measured and computed concentration profiles, and reads:

$$c_a = 0.015 \frac{d_{50} T^{1.5}}{a d_*^{0.3}} \quad (5.25)$$

The equilibrium concentration,  $\bar{c}_e$  in the advection-dispersion equations reads:

$$\bar{c}_e = 10^6 \cdot F \cdot C_a \cdot s \quad (5.26)$$

where  $F$  is a relation between the bottom concentration and the mean concentration based on numerical integration of the suspended concentration profile expressed by the ratio  $c/c_a$  previously mentioned, and  $s$  the relative density equal to 2.65.

If you use a scale factor,  $\bar{c}_e$  is multiplied with this factor.

### 5.3.4 Deposition

Deposition is described by:

$$S_d = -(\bar{c}_e - \bar{c}) \times w_s^*, \quad \bar{c}_e < \bar{c} \quad (5.27)$$

where  $w_s^*$  is a scaled fall velocity given by equation 5.7

### 5.3.5 Erosion

Similarly, erosion is described by:

$$S_e = -(\bar{c}_e - \bar{c}) \times w_s^*, \quad \bar{c}_e > \bar{c} \quad (5.28)$$

## 6 Hydrodynamic Variables

### 6.1 Bed Shear Stress

The sediment transport formulas described above apply hydrodynamic variables for describing the bed shear stress. This must be determined for pure current or a combined wave-current motion.

#### 6.1.1 Pure currents

In the case of a pure current motion the flow resistance is caused by the roughness of the bed. The bed shear stress under a current is calculated using the standard logarithmic resistance law:

$$\tau_c = \frac{1}{2} \rho f_c V^2 \quad (6.1)$$

Where:

$\tau_c$	bed shear stress (N/m <sup>2</sup> )
$\rho$	density of fluid (kg/m <sup>3</sup> )
$V$	mean current velocity (m/s)
$f_c$	current friction factor

$$f_c = 2 \left( 2.5 \left( \ln \left( \frac{30h}{k} \right) - 1 \right) \right)^{-2} \quad (6.2)$$

$h$	water depth (m)
$k$	bed roughness (m)

#### 6.1.2 Pure wave motion

In the case of pure wave motion, the mean bed shear stress reads:

$$\tau_w = \frac{1}{2} \rho f_w U_b^2 \quad (6.3)$$

Where:

$\tau_w$	bed shear stress
$f_w$	wave friction factor
$U_b$	horizontal mean wave orbital velocity at the bed (m/s)

$$U_b = \frac{2H_s}{T_z} \frac{1}{\sinh \left( \frac{2\pi}{L} h \right)} \quad (6.4)$$

$H_s$	significant wave height (m)
$T_z$	zero-crossing wave period (s)

An explicit approximation given by Swart (1974) for the wave friction factor is used:

$$\begin{aligned}
 f_w &= 0.47 & , & \quad \frac{a}{k} < 1 \\
 f_w &= \exp\left(5.213\left(\frac{a}{k}\right)^{-0.194} - 5.977\right) & , & \quad 1 < \frac{a}{k} \leq 3000 \\
 f_w &= 0.0076 & , & \quad \frac{a}{k} > 3000
 \end{aligned} \tag{6.5}$$

Where:

$a$  horizontal mean wave orbital motion at bed (m)

$$a = \frac{H_s}{\pi} \frac{1}{\sinh\left(\frac{2\pi}{L}h\right)} \tag{6.6}$$

An explicit expression of the wave length is given by Fenton and McKee (1990):

$$L = \frac{gT_z^2}{2\pi} \left( \tanh\left[\frac{2\pi}{T_z} \sqrt{\frac{h}{g}}\right]^{3/2} \right)^{2/3} \tag{6.7}$$

### 6.1.3 Combined currents and waves

Three wave-current shear stress formulations are offered.

#### Soulsby et al

Some of the formulations use a parameterised version of Fredsøe (1984) derived by Soulsby et al. 1993.

The default option for the parameterised model is to calculate and use the max shear stress. Other options are to calculate and use the mean shear stress or the RMS shear stress. The equations for mean shear stress, maximum shear stress and RMS shear stress are given below (Soulsby et al., 1993):

$$\begin{aligned}
 \frac{\tau_{mean}}{\tau_c + \tau_w} &= \frac{\tau_c}{\tau_c + \tau_w} \left(1 + b \left(\frac{\tau_c}{\tau_c + \tau_w}\right)^p \left(1 - \frac{\tau_c}{\tau_c + \tau_w}\right)^q\right) \\
 \frac{\tau_{max}}{\tau_c + \tau_w} &= 1 + a \cdot \left(\frac{\tau_c}{\tau_c + \tau_w}\right)^m \left(1 - \frac{\tau_c}{\tau_c + \tau_w}\right)^n \\
 \tau_{rms} &= \sqrt{\tau_{mean}^2 + 0.5 \cdot \tau_w^2}
 \end{aligned} \tag{6.8}$$

Where:

$\tau_c$  current alone shear stress

$\tau_w$  wave alone shear stress amplitude

$b, p, q, a, m, n$  constants, which vary for different wave-current theories parameterised

For the Fredsøe (1984) model, these constants are:

$$b = b_1 + b_2 |\cos \gamma|^j + (b_3 + b_4 |\cos \gamma|^j) \log_{10}(r)$$

$$p = p_1 + p_2 |\cos \gamma|^j + (p_3 + p_4 |\cos \gamma|^j) \log_{10}(r)$$

$$q = q_1 + q_2 |\cos \gamma|^j + (q_3 + q_4 |\cos \gamma|^j) \log_{10}(r)$$

$$a = a_1 + a_2 |\cos \gamma|^i + (a_3 + a_4 |\cos \gamma|^i) \log_{10}(r)$$

$$m = m_1 + m_2 |\cos \gamma|^i + (m_3 + m_4 |\cos \gamma|^i) \log_{10}(r)$$

$$n = n_1 + n_2 |\cos \gamma|^i + (n_3 + n_4 |\cos \gamma|^i) \log_{10}(r)$$

where  $a_1, a_2$ , etc. are given in the table below,  $\gamma$  is the angle between waves and currents,  $i = 0.8$ ,  $j = 3.0$  and  $r = 2 f_w / f_c$ .

Table 6.1 Constants for wave-current shear stress formulations

	<b>a</b>	<b>m</b>	<b>n</b>	<b>b</b>	<b>p</b>	<b>q</b>
1	-0.06	0.67	0.75	0.29	-0.77	0.91
2	1.70	-0.29	-0.27	0.55	0.10	0.25
3	-0.29	0.09	0.11	-0.10	0.27	0.50
4	0.29	0.42	-0.02	-0.14	0.14	0.45

## Fredsøe

A third option is to calculate and use the bed shear stress found from Fredsøe (1981).

For combined wave-current motion the eddy viscosity is strongly increased in the wave boundary layer close to the bed, and the near bed current profile is retarded.

The effect on the outer current velocity profile is described by introducing a “wave” roughness,  $k_w$ , which is larger than the actual bed roughness.

It is assumed that the wave motion is dominant close to the bed compared to the current, which means that the wave boundary layer thickness,  $\delta_w$ , and wave friction,  $f_w$ , can be determined by considering the wave parameters only. The wave boundary thickness,  $\delta_w$ , is found by (Johnsson and Carlsen, 1976):

$$\delta_w = 0.072k \left( \frac{a}{k} \right)^{0.75} \quad (6.9)$$

The velocity profile outside the wave boundary layer, which is influenced by the wave boundary layer is given by:

$$\frac{U(z)}{U_{fc}} = 2.5 \cdot \ln \left( \frac{30z}{k_w} \right) \quad (6.10)$$

Where:

$U(z)$	Velocity at vertical coordinate $z$ (m/s)
$U_{fc}$	Friction velocity (m/s)
$z$	vertical coordinate (m)
$k_w$	wave roughness

In case of weak wave motion, where the wave roughness  $k_w$  is less than the bed roughness  $k$  for pure current motion, the latter will be used.

The max bed shear stress for combined wave-current motion is given by:

$$\tau_b = \frac{1}{2} \rho f_w (U_b^2 + U_\delta^2 + 2U_b U_\delta \cos \alpha) \quad (6.11)$$

Where:

$U_\delta$	Current velocity at top ( $z = \delta_w$ ) of wave boundary layer
$\alpha$	Angle between mean current and direction of wave propagation

The resulting bed shear stress is found by the largest value of the bed shear stress for pure current derived by Equation (6.1) and the value derived by Equation (6.11).

## 6.2 Viscosity and Density

These two processes impact the HD-module by impacting the density and viscosity.

### 6.2.1 Mud impact on density

The influence from the mud on the water density is by definition given by:

$$\rho_m = \rho_w + \sum_i \left( 1 - \frac{\rho_w}{\rho_s} \right) c^i \quad (6.12)$$

### 6.2.2 Mud influence on viscosity

The influence on the kinematic viscosity from the mud can be parameterised by:

$$\frac{\nu_M}{\nu} = k_{v1}^{(a/k_{v2})} \quad (6.13)$$

Where  $k_{v1}$  and  $k_{v2}$  are calibration parameters and  $a = \sum_i c^i$ .

This expression is assumed to be valid for applying a lower limit for the eddy viscosity, hence:

$$\nu_T = \max(\nu_T, \nu_M) \quad (6.14)$$

Utilising

$$\frac{\nu_M}{\nu_T} = k_{v1}^{(a/k_{v2})} \quad (6.15)$$

## 7 Multi-Layer and Multi-Fraction Applications

### 7.1 Introduction

The MT model is a multi-layer and multi-fraction model. In the water column the mass concentrations  $c_1, c_2$ , etc. to  $c_i$  are defined. In the bed  $c_{1,1}, c_{2,1}$ , etc. to  $c_{i,1}$  are defined for the first layer and  $c_{1,2}, c_{2,2}$ , etc. to  $c_{i,2}$  for the second layer and consecutively. See also Figure 7-1.

Water column	Mass concentrations $c_1, c_2, \dots, c_i$
Bed layer 1	Dry density $c_{1,1}, c_{2,1}, \dots, c_{i,1}$
Bed layer 2	Dry density $c_{1,2}, c_{2,2}, \dots, c_{i,2}$
Bed layer n	Dry density $c_{1,n}, c_{2,n}, \dots, c_{i,n}$

Figure 7-1 Definition sketch for multi fractions-layers

The fractions are defined by their sediment characteristics. For the cohesive sediment fractions this gives the following extensions to the formulae above for deposition and erosion.

The deposition for the  $i$  mud fraction is:

$$D^i = w_s^i c_b^i p_D^i \quad (7.1)$$

where  $p_D^i$  is a probability ramp function of deposition:

$$p_D^i = \max \left( 0, \min \left( 1, 1 - \frac{\tau_b}{\tau_{cd}^i} \right) \right) \quad (7.2)$$

Erosion of the top layer of the bed is considered one incident calculated for one time step updating the sediment fraction ratio of the bed.

In the Mud Transport module, the sand transport description is based on the assumption that erosion takes place simultaneously for both sand and cohesive sediment. Therefore, the erosion of each layer is calculated using the normal mud transport erosion equations. Afterwards, the fraction of the sediment that may be kept in suspension under the present hydrodynamic conditions is calculated.

### 7.2 Dense Consolidated Bed

For a dense consolidated bed the erosion rate from the top layer  $j$ , can be calculated in the following way:

$$E_{j,total} = E_0^j p_E^{jE_m} \quad (7.3)$$

where  $p_E^j$  is a probability ramp function of erosion and  $E_0$  is the erodibility.

$$p_E^j = \max\left(0, \frac{\tau_b}{\tau_{ce}^j} - 1\right) \quad (7.4)$$

The erosion rate for the fraction  $i$  is then calculated as:

$$E_{i,j} = \frac{M_{i,j}}{M_{total,j}} E_{total}^j \quad (7.5)$$

in which  $M$  is the mass of sediment in the layer  $j$ .

### 7.3 Soft, Partly Consolidated Bed

Similarly for a soft, partly consolidated bed:

$$E_{total}^j = E_0^j \exp\left(\alpha^j (\tau_b - \tau_{ce}^j)^{0.5}\right) \quad (7.6)$$

The erosion rate for the fraction  $i$  is then calculated as:

$$E_{i,j} = \frac{M_{i,j}}{M_{total,j}} E_{total}^j \quad (7.7)$$

Each layer in the bed contains a certain concentration of sediment defined by a dry density excluding water content. This density is assigned the set of fractions applied. For example 60 percent particles < 63  $\mu\text{m}$  and 40 percent fine sand. This ratio is not fixed but can vary throughout the simulations, dependent on the advection-dispersion processes. An account is kept of the sediment ratios for the bed. This allows for a grain sorting process to take place.

## 8 Morphological Features

### 8.1 Morphological Simulations

The morphological evolution is sought to be included by updating the bathymetry for every time step with the net sedimentation rate. This ensures a stable evolution in the model that will not destabilise the hydrodynamic simulation.

$$bat^{n+1} = bat^n + nested^n \quad (8.1)$$

where

$bat^n$	Bathymetry at present time step
$bat^{n+1}$	Bathymetry at next time step
$n$	Time step

The Mud Transport module also allows the morphological evolution to be speeded up in the following way.

$$bat^{n+1} = bat^n + nested^n \textit{Speedup} \quad (8.2)$$

Speedup is a dimensionless factor. This factor is relevant for cases where the sedimentation processes are governed by cyclic events, such as tides or seasonal variation. This does NOT apply to stochastic events, such as storms.

The thickness of the individual bed layers is updated at the same time as the bathymetry. This is not the case for the suspended concentration.

### 8.2 Bed Update

The bed layer is updated using the following logistics (only 1 layer and 1 fraction is considered)

1. The net deposition is calculated as  $ND = \sum_{i=0}^I (D^i - E^i) \Delta t$
2. The bed mass  $M$  is calculated.
3. If net erosion occurs ( $ND > 0$ ) and  $M + ND < 0$ , the deposition and erosion rates are adjusted such that  $M + ND = 0$ .

4. The bed layer thickness,  $H$ , and density,  $\rho$ , are updated as:

$$H_{bed}^{new} = \begin{cases} H_{bed}^{old} + \frac{ND \cdot \Delta t}{\rho^i} & , \quad ND \leq 0 \\ H_{bed}^{old} + \frac{ND \cdot \Delta t}{\rho_{bed}^{old}} & , \quad ND > 0 \end{cases} \quad (8.3)$$

$$\rho_{bed}^{new} = \frac{H_{bed}^{old} \cdot \rho_{bed}^{old} + ND \cdot \Delta t}{H_{bed}^{new}} \quad (8.4)$$

## 9 Sediment Disposal

The simulation of disposal plumes from split barge is based on dynamic coupling of a nearfield integrated solution and the farfield mud transport model (MIKE 3 FM MT).

The behaviour of disposal material can be separated into three phases: Convective descent, during which the material falls under the influence of gravity; bottom collapse, occurring when the descending plume hits the bottom, and passive dispersion. The first two are so-called nearfield processes, where the dynamics and energy of the plume controls it. The last phase is the so-called farfield where the material transport and spreading are driven by ambient currents and turbulence.

### 9.1 Nearfield model theory

The nearfield model theory is mainly based on the model described by Johnson and Fong (1995), which is the theory behind the USACE STFATE model. Calculation of the convective descent phase follows the work of Koh and Chang (1973), where it is assumed that the material will retain a hemisphere shape with self-similar behaviour at all stages during convective descent (see Figure 9-1). The bed collapse phase follows the method introduced by Johnson and Fong (1995) which is based on conservation of energy.

The evolution of the plume in both phases is calculated based on the rate of entrainment and the sum of forces acting on the plume, including drag, buoyancy, bottom friction and the ambient currents.

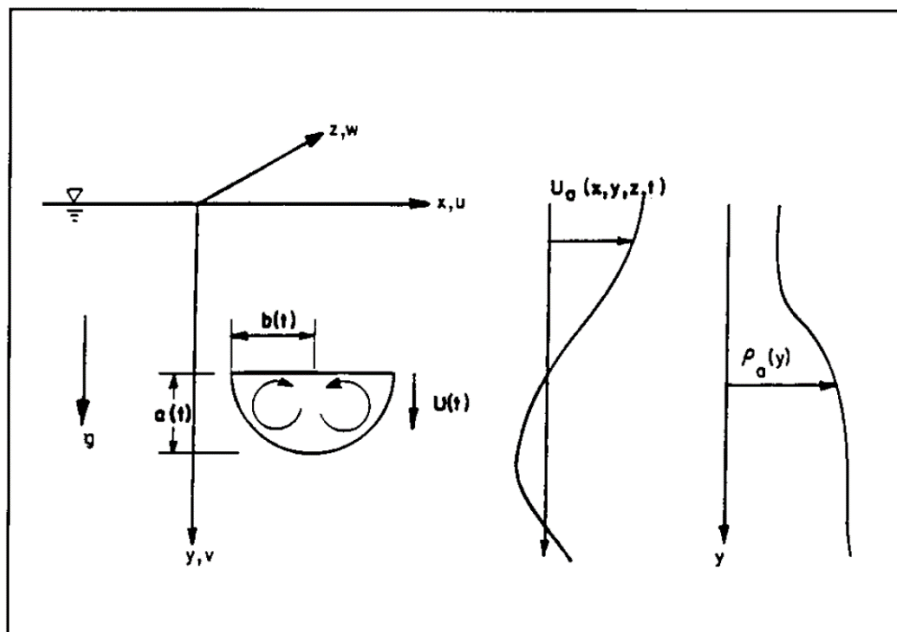


Figure 9-1 Convective descent, the hemispherical plume evolution under the ambient conditions (from Johnson and Fong, 1995)

The rate of change of volume (mass) in the plume during the convective descent is the rate of ambient fluid entrainment plus the possible fall-out of heavier fractions in the later stages of descent ( $q_{fall\ out}$ ) and stripping of sediment fractions ( $q_{strip}$ ).

$$\frac{dV}{dt} = E - \Sigma q_{fall\ out} - \Sigma q_{strip} \quad (9.1)$$

$V$  is the cloud volume calculated as  $V = \frac{2}{3}\pi b^3$  and  $E$  is the rate of entrainment, which is function of the plumes relative velocity to the ambient velocities, and the surface area of the hemispherical front.

$$E = 2\pi b^2 \alpha |\vec{U} - \vec{U}_a| \quad (9.2)$$

The entrainment coefficient  $\alpha$  is mainly dependent on the turbulence structure inside the plume. If the plume has a significant initial forcing (impulse), then it behaves as a vortex ring with small entrainment rates as function of vorticity and buoyancy (Turner, 1960). If it releases from rest, the plume behaves as a turbulent thermal and eventually (due to buoyancy force) large-scale circulation begins to develop inside the plume, increasing the vorticity and reducing the entrainment. It has been experimentally determined (Scorer, 1957 and Richards, 1961) that the entrainment coefficient for the turbulent thermals is around the constant value of  $\alpha = 0.25$ . Experiments of Ruggaber (2000) show that the variation (reduction) of entrainment coefficient from a turbulent thermal to a circulating thermal is less than 10%. In open water disposals, there is almost no forcing (impulse) involved in the initial evolution of the sediment plume, except the limited forcing (potential energy) due to material height inside the container. Therefore, following the value used in USACE STFATE model, the entrainment coefficient in MIKE Disposal module is set to constant value of 0.235.

In Johnson and Fong (1995) it is mentioned that according to Bokuniewicz, et al. (1978) the insertion speed of material (from the barge into the open water) is an important initial condition. Therefore, in MIKE Disposal module the plume insertion speed is included in the calculations.

The insertion speed mainly depends on barge dimensions and the opening area available for material exit. In order to simplify the calculations and reduce the unnecessary details, the barge characteristics is defined by four variables which combined with the disposal material characteristics are used to calculate the insertion speed:

- Overall area
- Inner area
- Opening area
- Unloaded draft

In Figure 9-2 the areal parameters are shown.

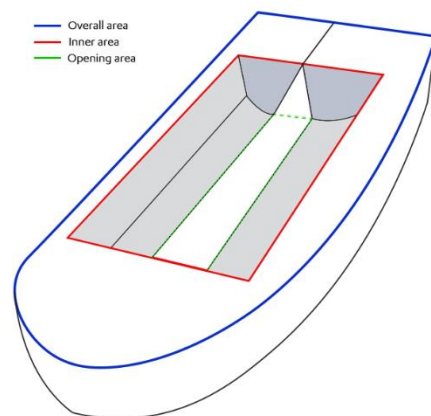


Figure 9-2 Definition of Vessel areal parameters

Plume insertion speed is calculated based on conservation of energy, described in the below equation. It varies in time as the material leave the barge.

$$V_{in} = \sqrt{\frac{2(\rho_m g h - \rho_a g h_d)}{\rho_m \left[ 1 + f/2 - \left( \frac{A_{opening}}{A_{inner}} \right)^2 \right]}} \quad (9.3)$$

$g$  is the gravitational acceleration,  $\rho_a$  is the ambient water density,  $\rho_m$  is the bulk density of material inside the barge,  $f$  is the friction coefficient at the barge opening set equal to 0.02 (Johnson and Fong, 1995),  $h$  is the height of material inside the barge, and  $h_d$  is the barge draft.

The plume momentum ( $M$ ) changes under the act of drag force ( $F_d$ ), buoyancy ( $F_b$ ) and rate of ambient fluid entrainment:

$$\frac{d\vec{M}}{dt} = \vec{F}_b + \vec{F}_d + E\rho_a\vec{U}_a \quad (9.4)$$

The buoyancy force is function of the plume density and its difference to ambient density. The plume density is function of the total sediment concentration and water salinity and temperature inside the plume.

$$F_b = \frac{2}{3}\pi b^3(\rho_m - \rho_a)\vec{g} \quad (9.5)$$

$$\rho_m = \sum c_i\rho_s + (1 - \sum c_i)\rho_w \quad (9.6)$$

$\rho_s$  is the sediment density,  $c_i$  is the volumetric concentration of  $i$ th sediment fraction and  $\rho_w$  is the density of water inside the plume, which is function of the salinity and temperature of the water inside the plume.

The drag force is calculated as below, where the drag coefficient is set to  $C_D = 1.0$  following the values in USACE STFATE model.

$$F_d = \frac{1}{2}\rho_a C_D \left( \frac{1}{2}\pi b^2 \right) U^2 \quad (9.7)$$

### 9.1.1 Sediment Stripping

As result of several factors, including turbulent shear, dynamics of the release, or high irregularities in material composition, some material is separated and left behind from the descending plume and remains in the water column. This so called "lost" or "stripped" material is transported out of the immediate site as passive plumes and is frequently viewed with concern under certain environmental conditions. Ruggaber (2000) did lab-scale experiments on release of sediment mixtures into stagnant ambient to study the stripping mechanisms. He concluded that the stem behind the descending plume is the main source of sediments stripping into the ambient as they left behind the main plume. In Figure 9-3 a snapshot of a released sediment mixture from a small-scale field study by Jensen et al. (2014) clearly shows the formation of the stem behind the main plume. Following the simplified approach used by Johnson and Fong (1995), the rate of sediment stripping from the plume is scaled with the plume area and its descending velocity.

$$q_{strp,i} = (2\pi b^2 C_{strp} U)(c_i) \quad (9.8)$$

The stripping coefficient  $C_{strp}$  is a calibration factor which reflects the local conditions and is left for the user to adjust. The default value of 0.0033 follows the default value given in

USACE STFATE. This default value of the stripping coefficient is selected so that approximately 2-5 percent of the total volume of fine material is stripped away at disposal sites of 30 meters or less. It is based upon field data collected by Bokuniewicz et al. (1978).

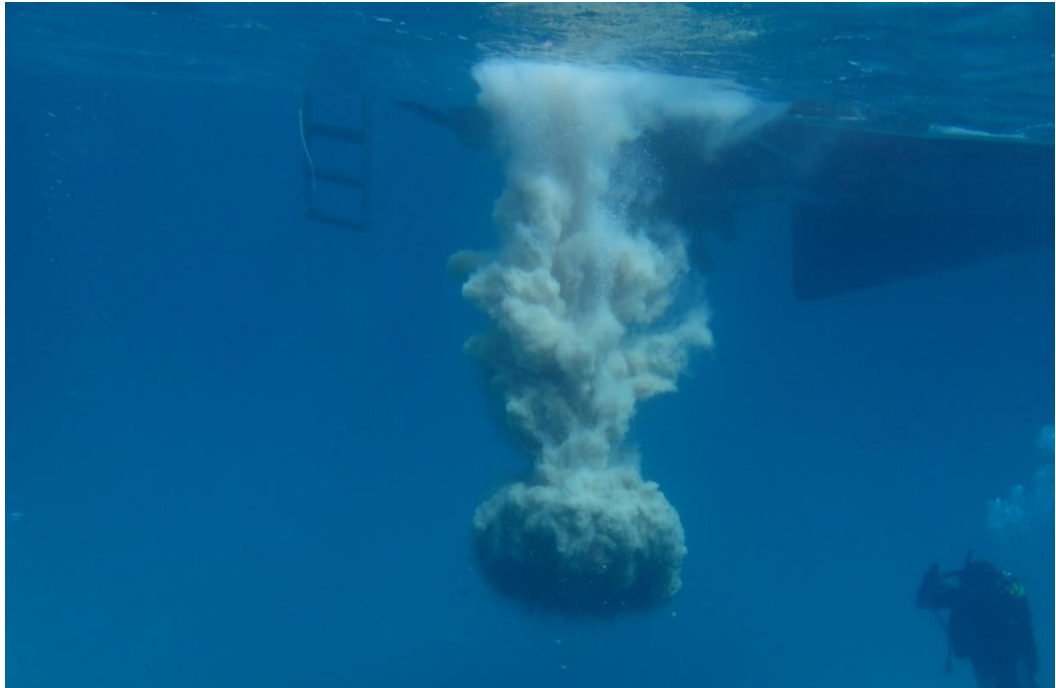


Figure 9-3 Snapshot of the descending plume from a small-scale field experiment (Jensen et al. 2014).

### 9.1.2 Sediment Fall-Out

If there is significant size difference between the sediment fractions in the plume (such as clumps), there is possibility for heavier fractions to fall out of the plume as soon as their individual fall velocity exceeds the plume's descending velocity. The descent velocity of plume is determined by its buoyancy. Meanwhile, the particles inside the cloud also fall with their own fall velocity, which is hindered due to high concentration inside the cloud. At later stages of the cloud's descent, as it gets diluted and slows down, the heavier fractions may fall out of it. The hindered settling velocity of each fraction inside the cloud is calculated as below:

$$w_{s,i} = w_{s0,i}(1 - \sum c_i)^n \quad (9.9)$$

$w_{s0,i}$  is the  $i$ th fraction's individual constant fall velocity (if flocculation is activated in the MT model setup then it will be the fall velocity at the onset of flocculation), and  $n$  is the hindered settling power coefficient which is calculated as function of sediment size, following the relation given by Garside and Al-Dibouni (1977).

In Figure 9-4 the laboratory experiment observations of Lai et al. (2016) on disposal of poly-disperse particle clouds is shown. The Letters represent particles of different diameter and settling velocity. In Figure 9-5 a photograph of the field experiment observations of Jensen et al. (2014) is shown, where the segregation and fall-out of the coarser fractions are clearly visible.

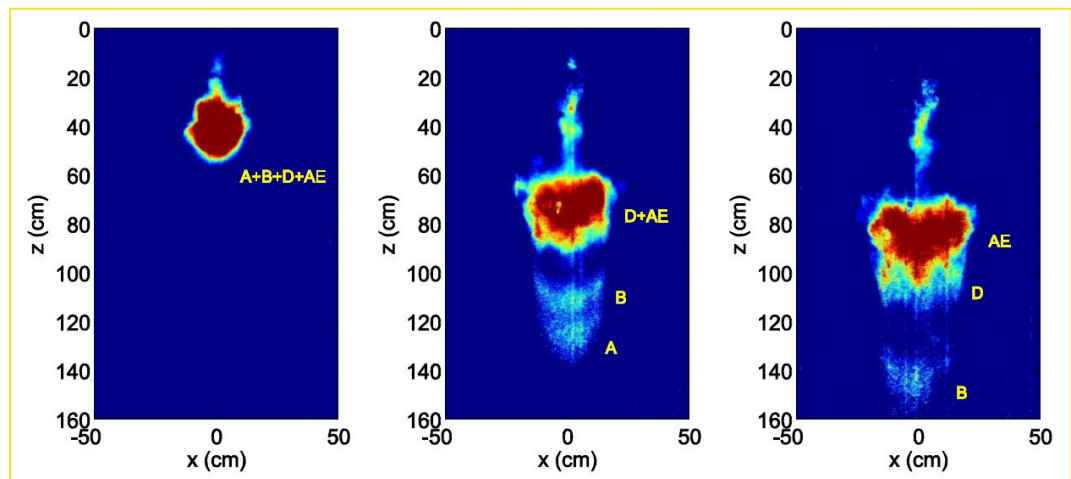


Figure 9-4 Typical observation in poly-disperse particle cloud experiments (ensemble averaged images at three points in time), from Lai et al. (2016).

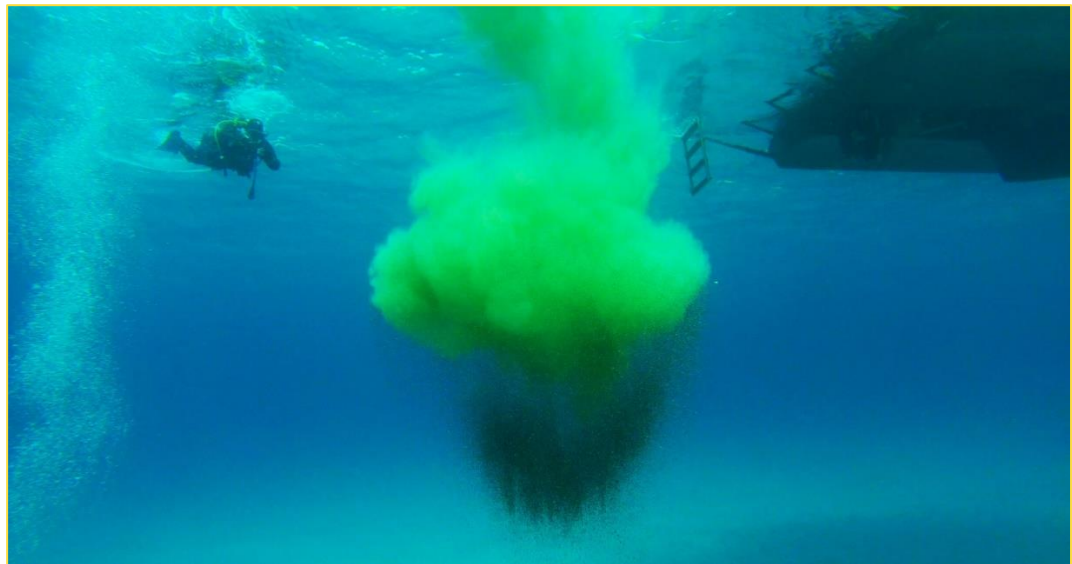


Figure 9-5 Field observation of disposal of poly-disperse particle clouds, from Jensen et al. (2014).

### 9.1.3 Dynamic Bed Collapse Phase

The bed collapse phase follows the method introduced by Johnson and Fong (1995) which is based on conservation of energy. When the cloud strikes the bottom, it possesses a certain amount of potential energy, which can be calculated since the mass of the cloud and the location of its centroid are known. In addition, the kinetic energy of the impacting cloud can be computed since its velocity is known. Thus, the total energy of the cloud at the time of impact is known. This energy is then available to drive the resulting bottom surge.

$$E_{K \text{ initial}} = \frac{1}{3} \rho \pi b^3 |\bar{U}|^2 \quad (9.10)$$

$$E_{P \text{ initial}} = \frac{3}{8} \Delta \rho g V b \quad (9.11)$$

The calculations are based on the assumption that the bottom collapsing cloud starts as one-half of an oblate spheroid (see Figure 9-6). The collapsing cloud dimensions are defined by its two horizontal radii ( $b_x$  and  $b_y$ ) and the vertical height ( $b_z$ ). In the beginning all radii equal the plume radius at the end of decent phase ( $b_x = b_y = b_z = b$ ).

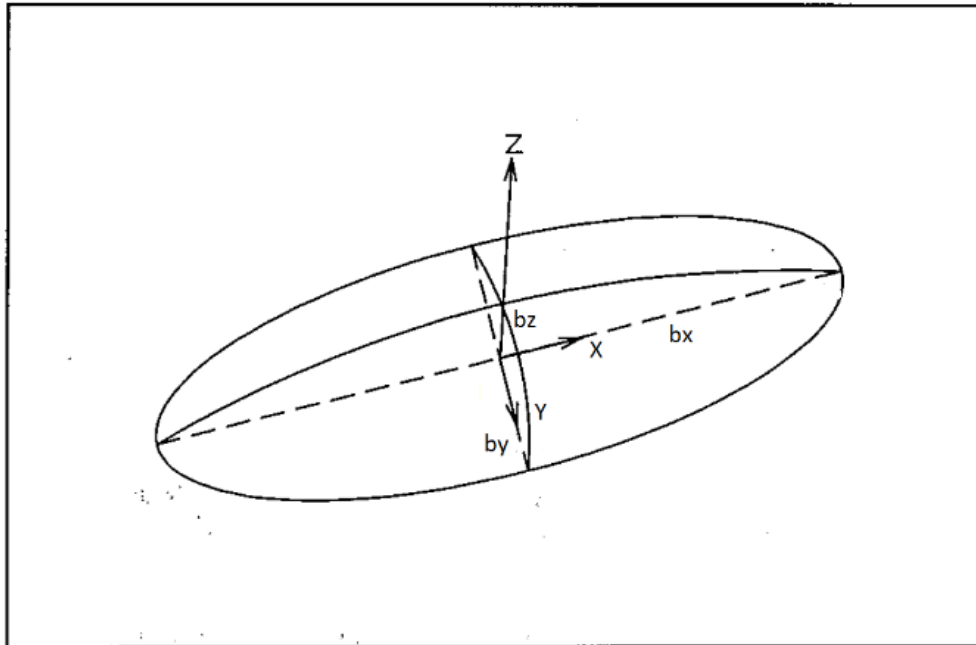


Figure 9-6 Dynamic Bottom Collapse is assumed to be an oblate spheroid (Johnson and Fong, 1995)

Considerably larger horizontal dimensions of the collapsing surge mean that different parts of the collapsing surge may experience different ambient conditions such as bottom slope, or interactions with land/boundaries. Therefore, similar to the approach used by Johnson and Fong (1995), the calculation of collapsing surge is done into four (4) quartals and each quartal may behave differently. In Figure 9-7 a snapshot of a collapsed plume just after seabed encounter is shown.

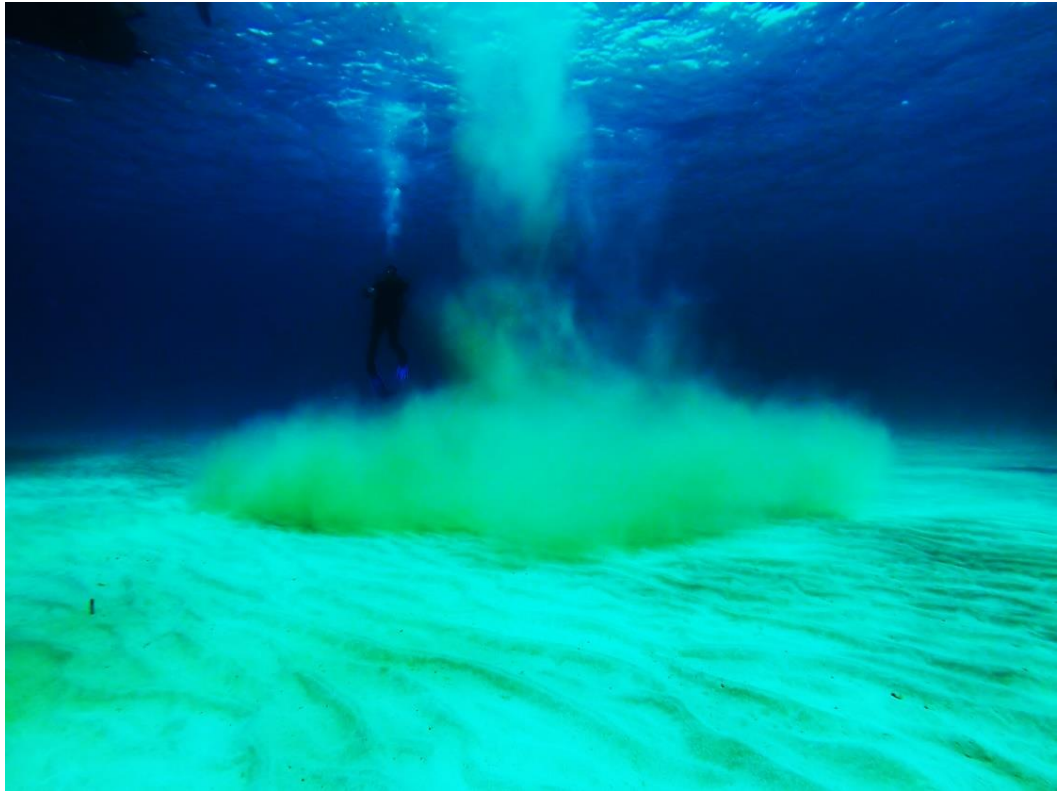


Figure 9-7 Collapse of sediment plume over the bed. From field observations by Jensen et al. (2014)

The collapse phase begins by calculating the change in the plume potential and kinetic energy based on work done to overcome bottom friction ( $W_{bf}$ ), drag ( $W_{drag}$ ), and the production of internal turbulence inside the surge ( $W_t$ ).

$$\Delta E_K + \Delta E_P = W_{total} \quad (9.12)$$

$$W_{total} = W_{bf} + W_{drag} + W_t + W_a \quad (9.13)$$

$$W_{bf} = \frac{1}{4} \rho_a C_{fr} \pi b_x b_y \left( \left( \frac{db_x}{dt} \right)^2 + \left( \frac{db_y}{dt} \right)^2 \right) \left( \sqrt{\left( \frac{db_x}{dt} \right)^2 + \left( \frac{db_y}{dt} \right)^2} \right) \Delta t \quad (9.14)$$

$$W_{drag} = \frac{1}{4} \rho_a C_{drag} \pi b_z \sqrt{b_x^2 + b_y^2} \left( \left( \frac{db_x}{dt} \right)^2 + \left( \frac{db_y}{dt} \right)^2 \right) \left( \sqrt{\left( \frac{db_x}{dt} \right)^2 + \left( \frac{db_y}{dt} \right)^2} \right) \Delta t \quad (9.15)$$

$$W_t = \frac{2}{3} \pi b_x b_y b_z \rho u_*^2 \frac{dv}{dz} \Delta t \quad (9.16)$$

$$u_* = 0.4 \frac{\sqrt{\left( \frac{db_x}{dt} \right)^2 + \left( \frac{db_y}{dt} \right)^2}}{\ln\left(\frac{b_z}{zz_0}\right)} \quad (9.17)$$

$$\frac{dv}{dz} = \frac{0.7 \sqrt{\left( \frac{db_x}{dt} \right)^2 + \left( \frac{db_y}{dt} \right)^2}}{b_z} \quad (9.18)$$

$u_*$  is the friction velocity and  $z_0$  is the seabed bottom roughness, as defined in the MT model setup. Bottom friction coefficient is set to  $C_{fr} = 0.001$ , and drag coefficient is set to  $C_{drag} = 0.1$  following the values in USACE STFATE model. Once the change in kinetic energy is known, the changes in cloud dimensions can be determined based on the following assumptions:

$$E_K = \frac{1}{10} \rho V \left[ \left( \frac{db_x}{dt} \right)^2 + \left( \frac{db_y}{dt} \right)^2 + \left( \frac{db_z}{dt} \right)^2 \right] \quad (9.19)$$

$$b_y \frac{db_y}{dt} = b_x \frac{db_x}{dt} \quad (9.20)$$

$$\frac{1}{b_x} \frac{db_x}{dt} + \frac{1}{b_y} \frac{db_y}{dt} + \frac{1}{b_z} \frac{db_z}{dt} = \frac{1}{V} \frac{dV}{dt} \quad (9.21)$$

$\frac{dV}{dt}$  is the change in the total volume of the cloud due to entrainment, stripping and settling out of sediments during the bottom surge.

Bottom slope is taken into account in the surge spreading calculations. The influence of a bottom slope is to increase the spread of the bottom surge in a downslope direction and to decrease the spread in an upslope direction. Following the simplified approach taken by Johnson and Fong (1995), the bottom slope at the centroid of each quartal is used to modify the spreading speed.

Entrainment rate and sediment stripping from the surge are scaled based on each quartal  $j$  frontal projected area, calculated as:

$$frontalArea_j = \frac{\pi}{4} b_z \sqrt{b_x^2 + b_y^2} \quad (9.22)$$

The entrainment coefficient and the stripping coefficient in the collapse phase are set similar as in the decent phase. Based on the friction velocity beneath the surge ( $u_*$ ) and the corresponding critical shear stress for deposition for each fraction (set in MT model), the rate of sedimentation underneath the surge is calculated. It should be noted that very fine sediments under very steep slopes may experience “auto-suspension”, a phenomenon that Bagnold (1962) described it well in details. The auto-suspension is not included in this Nearfield model, as it is a larger scale phenomenon outside dynamic collapse phase, governed by self-driven gravity currents on slopes.

## 9.2 Coupling of Nearfield model to MIKE FM

The nearfield model calculations including both decent and collapse phases are done during the same time step which the disposal occurs (as indicated in the vessel input file). The placement of sediments either in suspension or deposition also occur in the same time step.

During the decent phase the plume can become passive if:

- Plume momentum falls below ambient momentum
- Plume gets trapped in a density layer due to dilution in stratified ambient

If the plume becomes passive during the descent phase, sediment mass is released into water column as suspended sediment in a circular plane corresponding to the plume size at the moment of release.

During the collapse phase each plume quartal can become passive if:

- Plume quartal momentum falls below ambient momentum based on velocity or density
- Plume quartal becomes diffusive under high energy bed impacts

If each of the plume quartals become passive during the collapse phase, sediment mass is released into water column as suspended sediment over a 3D volume corresponding to the quartal's dimensions at the moment of release.

During both the descent and the collapse phase the stripped sediments are released into water column as suspended sediment into individual points corresponding to the location of the centre of mass of the plume at the moment the stripped volume is calculated.

During the descent phase, in case a sediment fraction falls out of the plume, the fall-out mass of sediment is placed into the first bed layer as deposited sediment, covering an area corresponding to the size of the plume at the moment of fall-out.

The depositing sediment during the collapse phase is placed into the first bed layer as deposited sediment, covering an area corresponding to the dimensions of the plume at the moment it is calculated.

In case the release of plume occurs close to land or an open boundary, and part of it falls out of the domain, the sediment mass corresponding to that part is placed at the closest cell inside the domain.

In Figure 9-8 and Figure 9-9 the above described processes are depicted in schematic drawings. In Figure 9-10 an example of Disposal plume coupling with MIKE FM is shown.

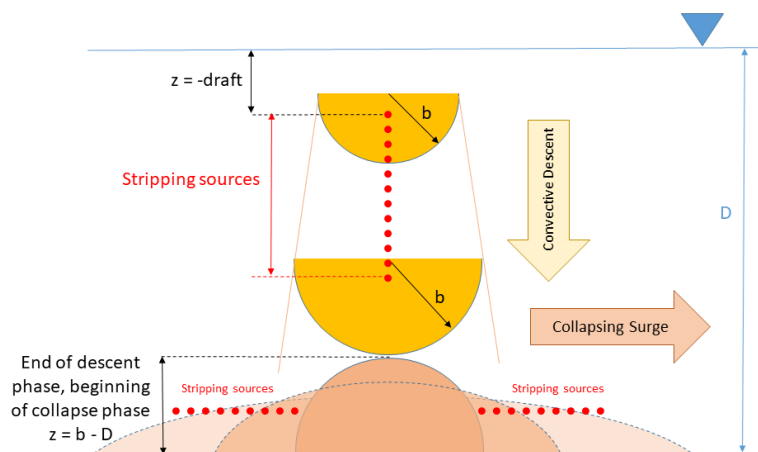


Figure 9-8 Schematic description of the nearfield model definitions

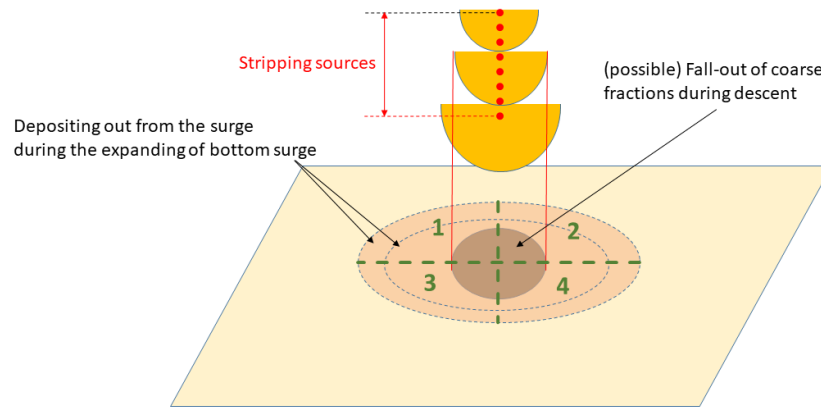


Figure 9-9 Deposition into the seabed may occur due to fall out during convective descent or during the surge spreading

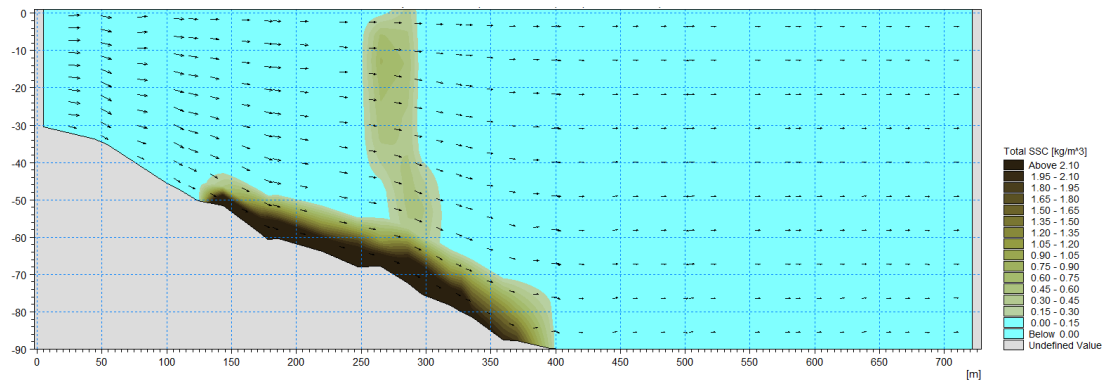


Figure 9-10 An example Disposal module results in MIKE3 FM. The stripped sediments are placed in water column, and the collapse plume placed over the seabed after becoming passive

## 10 Propeller wash

The excess shear stress imposed on seabed due to the vessel's propeller wash is calculated by nearfield sub-model which approximates the jet flow field resulted from the propeller efflux by analytical equations based on conservation of mass and momentum. The calculated shear stress field is added to the existing shear stress field in sediment transport model at each time step.

### 10.1 Nearfield model theory

The flow velocity leaving the propeller is determined by the 'actuated disc' theory also known as the momentum theory, which simply assumes that there is a pressure difference between the upstream and the downstream side at the plane of the propeller.

Theoretical development of the equation used to predict the efflux velocity  $V_0$  of a propeller is based on axial momentum theory and is shown in equation (10.1). This equation is widely investigated by several researchers such as Hamill et. al. (1989) and Berger et. al. (1981).

$$V_0 = 1.59nD_p\sqrt{K_T} \quad (10.1)$$

$K_T$  is the propeller thrust coefficient,  $D_p$  is the propeller diameter, and  $n$  is the number of revolutions per second of the propeller. The coefficient 1.59 might not be constant. It is changeable based on the propeller characteristics. Here however it has been set as constant, considering that 1) propeller wash sub-model is a simplistic/approximative approach not meant for detailed design analysis, 2) there are many other uncertainties involved in calculations, and 3) usually such detailed information on propeller is not available.

When the ship is in motion, the calculation of efflux velocity  $V_0$  should be modified in three steps: 1) the velocity of the approaching water has to be estimated, 2) the combined velocity field of the propeller jet and the wake behind the ship has to be found and 3) transformation from the velocities relative to the ship to velocities relative to the seabed.

The approach velocity  $U_{App}$  of the water flowing to the propeller is determined by: 1) the sailing speed,  $U_{sail}$ , of the ship, 2) the return current,  $U_r$ , which may be generated when sailing in restricted waters (the return current is not considered further in the following) and 3) the effect of the wake described by a wake coefficient  $w$ . The approach velocity is thus given as:

$$U_{App} = (U_{sail} + U_r)(1 - w) \quad (10.2)$$

The wake coefficient can, as a first approximation, be estimated as:

$$w = -0.05 + 0.5C_B \quad (10.3)$$

$C_B$  is the block coefficient determined as the ratio between the displaced volume of the ship and the volume of the smallest box in which the ship can float. For larger bulk carriers and tank ships  $C_B$  is about 0.8-0.85 (see Kristensen (2012)), while it is somewhat smaller for most other types of ships.

The efflux velocity from the moving vessel propeller  $V_{0m}$  can be calculated as:

$$V_{0m} = \sqrt{u_A^2 + V_0^2} \quad (10.4)$$

The propeller speed,  $n$ , must be estimated for the actual sailing speed. As a first approximation it may be estimated from the design conditions for the sailing velocity and propeller rotation assuming that the propeller rotation is proportional to the sailing speed

(and that the power delivered by the machine is proportional to the sailing speed raised to a power of 3).

The flow behind the propeller is divided into four zones (see Figure 10-1):

1. Zone of flow establishment
2. Zone of established flow (free turbulent jet)
3. Attachment zone
4. Wall jet

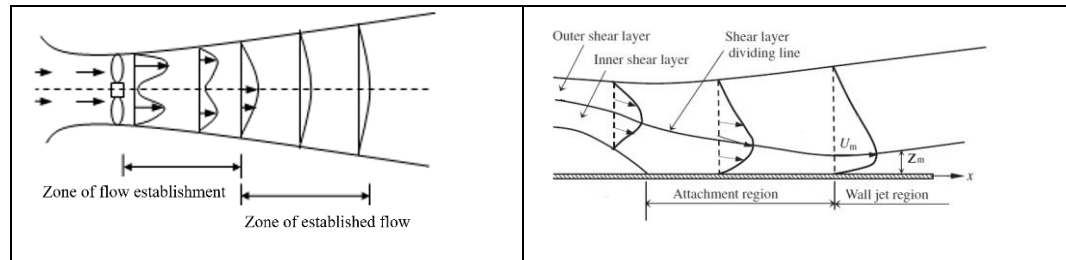


Figure 10-1 Left: Sketch of zone of flow establishment & zone of established flow behind the propeller (Image adopted from Lam et. al (2005)), Right: Sketch of the attachment (to seabed) region and wall-jet region downstream the propeller (Image adopted from Agelin-Chaab et. al. (2011)).

The zone of flow establishment is the region where the jet was divided into two parts by the influence of the rotating hub. Steward (1995) states the zone of flow establishment ranges from the efflux plane to  $3.25D_p$ .

Here it is assumed that by the end of the zone of flow establishment, the jet flow has a Gaussian distribution, with total flux equivalent to:

$$Q_0 = \pi \frac{D_p^2}{4} V_{0m} \tag{10.5}$$

In the zone of established flow the solution is based on the integral jet model equations described by Jirka (2004). It determines the steady state solution of the jet/plume by solving conservation equations for flux and momentum, salinity and temperature (if included) under the given ambient conditions.

The velocity profile and distribution of state parameters and scalar mass is assumed to follow the Gaussian formulation. The jet model employs an entrainment closure approach that distinguishes between the separate contributions of transverse shear and of azimuthal shear mechanisms. It further contains a quadratic law turbulent drag force mechanism ( $F_D$ ) as suggested by a number of recent detailed experimental investigations on the dynamics of transverse jets into crossflow. The conservation principles for volume (continuity), momentum components in the global directions, state parameters and scalar mass, follow Jirka (2004), lead to the equations below:

$$\frac{dQ}{ds} = E \tag{10.6}$$

$$\frac{dM_x}{ds} = E u_a + F_D \sqrt{1 - \cos^2 \theta \cos^2 \sigma} \tag{10.7}$$

$$\frac{dM_y}{ds} = -F_D \frac{\cos^2 \theta \sin \sigma \cos \sigma}{\sqrt{1 - \cos^2 \theta \cos^2 \sigma}} \tag{10.8}$$

$$\frac{dM_z}{ds} = \pi\lambda^2 b^2 g'_c - F_D \frac{\sin\theta \cos\theta \cos\sigma}{\sqrt{1 - \cos^2\theta \cos^2\sigma}} \tag{10.9}$$

Where  $s$  is the axial distance along the jet trajectory and  $E$  is the rate of entrainment, and  $b$  is the characteristic width of the jet, which is defined as the jet radius, where the jet excess velocity is  $e^{-1} = 37\%$ .

After a certain distance depending on the clearance from seabed, the jet flow begins to interact with seabed. The jet curves towards the seabed due to reduction in pressure, also known as the Coanda effect. The extent of the attachment zone depends on the initial clearance and the jet characteristics. However, it is typically a few (initial) jet diameters. At the end of the attachment zone the flow converts into a full 3-dimensional wall-jet. Here, the attachment zone is ignored due to its limited extent and the complex processes involved in it which are not crucial for the purpose of this sub-model. It is assumed that as soon as the lower boundaries of the jet flow touches the seabed, it converts into wall-jet.

The wall jet is considered to comprise two parts: an inner flow adjacent to the wall having a highly non-linear velocity profile characteristic of a turbulent wall flow, and an outer flow having a velocity profile more typical of a free turbulent plane jet.

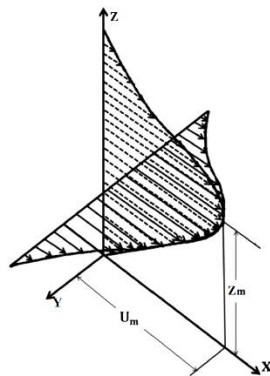


Figure 10-2 3-dimensional velocity profile of wall-jet (Image adopted from Kheirkhah et. Al. (2014))

The 3-dimensional velocity profile at point  $x$  along the trajectory is defined as:

$$U = u_c f(y) g(z) \tag{10.10}$$

The functions  $f$  and  $g$  define vertical and transverse variations in the velocity profile. The parameter  $u_c$  is the maximum centreline velocity of the jet.

The transverse velocity profile is assumed to be similar to free turbulent jets, and takes the Gaussian form:

$$f(y) = e^{-\frac{y^2}{b_h^2}} \tag{10.11}$$

where  $b_h$  is the characteristic horizontal width of the jet. Following Roberts (1986), the vertical velocity profile is considered to comprise two parts: an inner flow adjacent to the wall having a highly non-linear velocity profile characteristic of a turbulent wall flow, and an outer flow having a velocity profile more typical of a free turbulent jet. These two profiles join at maximum jet centreline velocity at  $z = z_m$ , which is defined by:

$$z_m = \frac{b_v}{1+7k} \tag{10.12}$$

where  $b_v$  is the vertical jet characteristic width in the outer flow jet, and  $k = 0.8814$ .

$$g(z) = \begin{cases} 2 \left( \frac{z}{z_m} \right)^{\frac{1}{7}} - \left( \frac{z}{z_m} \right)^{\frac{2}{7}}, & z < z_m \\ \operatorname{sech}^2 \left( \frac{k(z-z_m)}{b_v-z_m} \right), & z \geq z_m \end{cases} \quad (10.13)$$

The outer flow free turbulent jet velocity profile is modified to give  $U = U_{max}$  at  $z = z_m$ .

Flux and momentum equations for wall jet will be a combination of the outer and inner flow:

$$\begin{aligned} Q &= \int_{-\infty}^{\infty} \left( \int_0^{z_m} U_{inner} dz + \int_{z_m}^{\infty} U_{outer} dz \right) dy = \int_{-\infty}^{\infty} u_c e^{-\frac{y^2}{b_h^2}} \left( \left( \frac{7}{4z_m^{\frac{1}{7}}} Z^{\frac{8}{7}} - \frac{7}{9z_m^{\frac{2}{7}}} Z^{\frac{9}{7}} \right)_{z=0}^{z_m} + \right. \\ &\left. \left( \frac{(b_v-z_m)}{k} \tanh \left( \frac{k(z-z_m)}{(b_v-z_m)} \right) \right)_{z=z_m}^{\infty} \right) dy = \int_{-\infty}^{\infty} u_c e^{-\frac{y^2}{b_h^2}} \left( \left( \frac{35}{36} z_m \right) + \left( \frac{(b_v-z_m)}{k} \right) \right) dy = \\ &u_c b_h \sqrt{\pi} \left( \left( \frac{35}{36} z_m \right) + \left( \frac{(b_v-z_m)}{k} \right) \right) \end{aligned} \quad (10.14)$$

$$\begin{aligned} M &= \int_{-\infty}^{\infty} \left( \int_0^{z_m} U_{inner}^2 dz + \int_{z_m}^{\infty} U_{outer}^2 dz \right) dy = \int_{-\infty}^{\infty} \left( \int_0^{z_m} \left( u_c^2 e^{-\frac{2y^2}{b_h^2}} \left( 4 \left( \frac{z}{z_m} \right)^{\frac{2}{7}} + \left( \frac{z}{z_m} \right)^{\frac{4}{7}} - \right. \right. \right. \\ &\left. \left. \left. 4 \left( \frac{z}{z_m} \right)^{\frac{3}{7}} \right) dz + \int_{z_m}^{\infty} \left( u_c^2 e^{-\frac{2y^2}{b_h^2}} \operatorname{sech}^4 \left( \frac{k(z-z_m)}{(b_v-z_m)} \right) \right) dz \right) dy = \int_{-\infty}^{\infty} u_c^2 e^{-\frac{2y^2}{b_h^2}} \left( \left( \frac{28}{9z_m^{\frac{9}{7}}} + \right. \right. \\ &\left. \left. \frac{7}{11z_m^{\frac{4}{7}}} Z^{\frac{11}{7}} - \frac{28}{10z_m^{\frac{10}{7}}} Z^{\frac{10}{7}} \right)_{z=0}^{z_m} + \left( \frac{(b_v-z_m)}{k} \left( \tanh \left( \frac{k(z-z_m)}{(b_v-z_m)} \right) - \frac{1}{3} \tanh^3 \left( \frac{k(z-z_m)}{(b_v-z_m)} \right) \right) \right)_{z=z_m}^{\infty} \right) dy = \\ &\int_{-\infty}^{\infty} u_c^2 e^{-\frac{2y^2}{b_h^2}} \left( \left( \frac{938}{990} z_m \right) + \left( \frac{2(b_v-z_m)}{3k} \right) \right) dy = u_c^2 b_h \sqrt{\frac{\pi}{2}} \left( \left( \frac{938}{990} z_m \right) + \left( \frac{2(b_v-z_m)}{3k} \right) \right) \end{aligned} \quad (10.15)$$

It is assumed that the cross-sectional area of the wall jet has an oval shape, with different horizontal and vertical spreading rates following the assumption:

$$\frac{db_h}{ds} \approx 5 \frac{db_v}{ds} \quad (10.16)$$

From here, the equations of conservation of momentum and flux are solved in a similar fashion as the free jet section, with the addition of bed friction as an extra opposing force. The wall-jet calculations cease as soon as the jet momentum drops below the ambient momentum, or it exceeds the user-defined maximum travelling distance.

## 10.2 Bed shear stress caused by propeller induced jet flow over seabed

The bed shear stress over the areal extent of the attached jet flow (wall-jet) is calculated by two methods:

1. Simple log-law assumption
2. Advanced moving turbulent boundary layer assumption

### 10.2.1 Simple log-law assumption

It is assumed that the inner flow profile of the wall-jet comprises a fully turbulent log profile, with  $u_c$  (maximum jet centreline velocity) as an approximate for the mean velocity in the log profile:

$$\tau_b = \left( \frac{u_c}{6.1 - 2.5 \ln\left(\frac{kn}{zm}\right)} \right)^2 \tag{10.17}$$

### 10.2.2 Advanced moving turbulent boundary layer assumption

This method applies only to moving vessels where the propeller induced shear stress over seabed is not steady, so that the generation of the turbulent boundary layer underneath the wall-jet is dynamic. A solution similar to that of the wave boundary layers is applied in this case to calculate the bed shear stress.

## 10.3 Coupling of Nearfield model to MIKE FM

The calculated bed shear stress fields at each computational time step is projected into the MIKE FM solution as an excess shear stress added to the ambient bed shear stress calculated by the hydrodynamic model. In Figure 10-3 an example of bed shear stress from propeller wash is shown

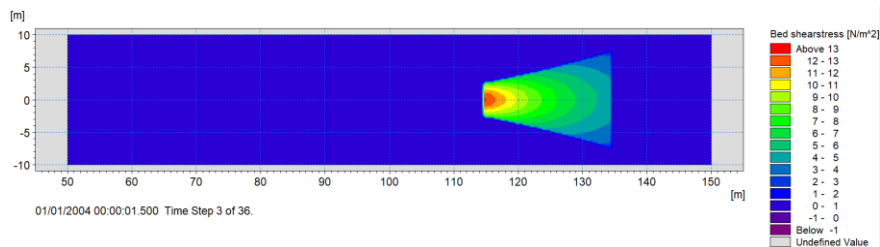


Figure 10-3 Example of excess bed shear stress due to propeller wash

## 11 References

- /1/ Agelin-Chaab, M. and Tachie, M.F., 2011. Characteristics and structure of turbulent 3D offset jets. *International Journal of Heat and Fluid Flow*, 32(3), pp.608-620.
- /2/ Andersen, T.J., 2001. Seasonal variation in erodibility of two temperate microtidal mudflats. *Estuarine, Coastal and Shelf Science* 56, pp 35-46
- /3/ Andersen, T.J. & Pejrup, M., 2001. Suspended sediment transport on a temperate, microtidal mudflat, the Danish Wadden Sea. *Marine Geology* 173, pp 69-85
- /4/ Bagnold, R.A., 1962. Auto-suspension of transported sediment; turbidity currents. *Proceedings of the Royal Society of London. Series A. Mathematical and Physical Sciences*, 265(1322), pp.315-319.
- /5/ Berger, W., Felkel, K., Hager, M., Oebius, H. and Schale, E., 1981, May. Courant provoqué par les bateaux protection des berges et solution pour éviter l'érosion du lit du haut rhin. In PIANC, 25th Congress, Section I-1. Edinburgh.
- /6/ Bokuniewicz, H.J., 1978. Field study of the mechanics of the placement of dredged material at open-water disposal sites (Vol. 1). *Waterways Experiment Station*.
- /7/ Burt, T.N., 1986. Field settling velocities of estuary muds. In *Estuarine Cohesive Sediment Dynamics. Lecture Notes on Coastal and Estuarine Studies*. (Mehta, A.J., ed.). Springer Verlag, Berlin, pp 126-150.
- /8/ Delo, E.A., Ockenden, M.C., 1992. "Estuarine Muds Manual" HR Wallingford, Report SR309, May 1992.
- /9/ Dyer, K.R., 1986. *Coastal and Estuarine Sediment Dynamics*. John Wiley & Sons, pp 342.
- /10/ Edelvang, K. & Austen, I., 1997. The temporal variation of flocs and fecal pellets in a tidal channel. *Estuarine, Coastal and Shelf Science* 44, 361-367.
- /11/ Eisma, D., 1993. *Suspended matter in the aquatic environment*. Springer Verlag, pp 315.
- /12/ Ekebjærg, L. and Justesen, P., 1991. "An Explicit Scheme for Advection-Diffusion Modelling in Two Dimensions". *Comp. Meth. App. Mech. Eng.*, pp. 287-297.
- /13/ Engelund, F., Fredsøe, J., 1976. "A sediment transport model for straight alluvial channels". *Nordic Hydrology* 7, pp. 293 - 306.
- /14/ Fenton and McKee, 1990. "On Calculating the Lengths of Water Waves". *Coastal Engineering*, Vol. 14, Elsevier Science Publishers BV, Amsterdam, pp. 499-513.

- /15/ Fredsøe, J., 1981.  
"Mean Current Velocity Distribution in Combined Waves and Current". Progress Report No. 53, ISVA, Technical University of Denmark.
- /16/ Fredsøe, J., 1984.  
"Turbulent boundary layer in wave-current motion". J Hydr Eng, A S C E, Vol 110, HY8, 1103-1120.
- /17/ Garside, J. and Al-Dibouni, M.R., 1977. Velocity-voidage relationships for fluidization and sedimentation in solid-liquid systems. Industrial & engineering chemistry process design and development, 16(2), pp.206-214.
- /18/ Gibbs, R.J. 1985.  
Estuarine flocs: Their size, settling velocity and density. Journal of Geophysical Research 90, pp 3249-3251.
- /19/ Grishanin, K.V, and Lavygin, A.M., 1987.  
"Sedimentation of dredging cuts in sand bottom rivers". PIANC, Bulletin, No. 59, pp. 50-55.
- /20/ Hamill, G.A., 1989. Characteristics of the screw wash of a manoeuvring ship and the resulting bed scour.
- /21/ Jensen, J.H., Saremi, S., Jimenez, C. and Hadjioannou, L., 2015. Field experimental observations of highly graded sediment plumes. Marine pollution bulletin, 95(1), pp.72-80.
- /22/ Jirka, G.H., 2004. Integral model for turbulent buoyant jets in unbounded stratified flows. Part I: Single round jet. Environmental fluid mechanics, 4(1), pp.1-56.
- /23/ Johnson, B.H. and Fong, M.T., 1995. Development and Verification of Numerical Models for Predicting the Initial Fate of Dredged Material Disposed in Open Water. Report 2. Theoretical Developments and Verification Results. ARMY ENGINEER WATERWAYS EXPERIMENT STATION VICKSBURG MS.
- /24/ Jonsson, I.G. and Carlsen, N.A., 1976.  
"Experimental and Theoretical Investigations in an Oscillatory Rough Turbulent Boundary Layer". J. Hydr. Res. Vol. 14, No. 1, pp. 45-60.
- /25/ Kheirkhah Gildeh, H., Mohammadian, A., Nistor, I. and Qiblawey, H., 2014. Numerical modeling of turbulent buoyant wall jets in stationary ambient water. Journal of Hydraulic Engineering, 140(6), p.04014012.
- /26/ Koh, R.C.Y. and Chang, Y.C., 1973. Mathematical Model for Barged Ocean Disposal of Wastes. Environmental Protection Technology Series WPA-660.
- /27/ Kristensen, H.O., 2012. Determination of regression formulas for main dimensions of tankers and bulk carriers based on IHS Fairplay data. Clean Shipping Currents, 1(6).
- /28/ Krone, R.B., 1962.  
"Flume Studies of the Transport of Sediment in Estuarial Processes". Hydraulic Engineering Laboratory and Sanitary Engineering Research Laboratory, Univ. of California, Berkely, California, Final Report.
- /29/ Krone, B. 1986.  
The significance of aggregate properties to transport processes. In: Mehta A.J. (Ed) Estuarine Cohesive Sediment Dynamics, Springer Verlag, pp. 66-84.

- /30/ Lam, W.H., Hamill, G., Robinson, D., Raghunathan, R. and Kee, C., 2005. Submerged propeller jet. In WSEAS Conferences, Udine, Italy (pp. 491-218).
- /31/ Lai, A.C., Wang, R.Q., Law, A.W.K. and Adams, E.E., 2016. Modeling and experiments of polydisperse particle clouds. *Environmental Fluid Mechanics*, 16(4), pp.875-898.
- /32/ Leonard, B.P., 1979. "A stable and accurate convective modelling procedure based on quadratic upstream interpolation". *Comput. Meths. Appl. Mech. Eng.* 19, pp. 59-98.
- /33/ Leonard, B.P., 1991. "The ULTIMATE Conservative Differential Scheme Applied to Unsteady One-Dimensional Advection". *Comput. Meths. Appl. Mech. Eng.* 88, 17-74.
- /34/ Mehta, A.J., Hayter, E.J., Parker, W.R., Krone, R.B., Teeter, A.M., 1989. "Cohesive Sediment Transport. I: Process Description". *Journal of Hydraulic Eng.*, Vol. 115, No. 8, Aug. 1989, pp. 1076-1093.
- /35/ Parchure, T. M. and Mehta, A.J., 1985. Erosion of soft cohesive sediment deposits. *Journal of Hydraulic Engineering - ASCE* 111 (10), 1308-1326.
- /36/ Partheniades, E., 1965. Erosion and deposition of cohesive soils. *Journal of the Hydraulics Division Proceedings of the ASCE* 91 (HY1), 105-139.
- /37/ Pejrup, M., 1988a. Flocculated suspended sediment in a micro-tidal environment. *Sedimentary Geology* 57, 249-256.
- /38/ Pejrup, M., Larsen, M. and Edelvang, K., 1997. A fine-grained sediment budget for the Sylt-Rømø tidal basin. *Helgoländer Meeresuntersuchungen* 51, 1-15.
- /39/ Postma, H., 1967. "Sediment Transport and Sedimentation in the Estuarine Environment". In: Lauff G.H: (Ed) *Estuaries AAAS Publ.* 83, p 158-179
- /40/ Richards, J.M., 1961. Experiments on the penetration of an interface by buoyant thermals. *Journal of Fluid Mechanics*, 11(3), pp.369-384.
- /41/ Rijn, L.C., 1984. "Sediment Transport, Part I Bed Load Transport". *Journal of Hydraulic Engineering*, Vol. 110, No. 10, October, 1984.
- /42/ Rijn, L.C., 1984. "Sediment Transport, Part II Suspended Load Transport". *Journal of Hydraulic Engineering*, Vol. 110, No. 10, October, 1984.
- /43/ Rijn, Van L.C., 1989. "Handbook on Sediment Transport by Current and Waves". *Delft Hydraulics, Report H461*, June 1989, pp. 12.1-12.27.
- /44/ Roberts, L., 1986, March. A theory for turbulent curved wall jets. In 25th AIAA Aerospace Sciences Meeting (p. 4).

- /45/ Ruggaber, G.J., 2000. Dynamics of particle clouds related to open-water sediment disposal (Doctoral dissertation, Massachusetts Institute of Technology).
- /46/ Sanford, L.P. and Maa, J.P., 2001.  
A unified erosion formulation for fine sediments. *Marine Geology* 179 (1-2), 9-23.
- /47/ Scorer, R.S., 1957. Experiments on convection of isolated masses of buoyant fluid. *Journal of Fluid Mechanics*, 2(6), pp.583-594.
- /48/ Soulsby R.L., Hamm L., Klopman G., Myrhaug D., Simons R.R., and Thomas G.P., 1993.  
"Wave-current interaction within and outside the bottom boundary layer". *Coastal Engineering*, 21, 41-69.
- /49/ Stewart, D.P.J., 1995. Characteristics of a ship's screw wash and the influence of quay wall proximity.
- /50/ Swart, D.H., 1974.  
"Offshore sediment transport and equilibrium beach profiles". Delft Hydr. Lab. Publ., 1312, Delft Univ. technology Diss., Delft.
- /51/ Teeter, A.M., 1986.  
"Vertical Transport in Fine-Grained Suspension and Nearly-Deposited Sediment". *Estuarine Cohesive Sediment Dynamics, Lecture Notes on Coastal and Estuarine Studies*, 14, Springer Verlag, pp. 126-149.
- /52/ Teisson, C., 1991.  
"Cohesive suspended sediment transport: feasibility and limitations of numerical modelling". *Journal of Hydraulic Research*, Vol. 29, No. 6.
- /53/ Turner, J.S., 1960. A comparison between buoyant vortex rings and vortex pairs. *Journal of Fluid Mechanics*, 7(3), pp.419-432.
- /54/ US Environmental Protection Agency, 1994. Evaluation of dredged material proposed for discharge in waters of the US—Testing manual.
- /55/ Van Leussen, W. 1988.  
Aggregation of particles, settling velocity of mud flocs. A review: In: Dronkers & Van Leussen (Eds.): *Physical processes in estuaries*. Springer Verlag, pp 347-403.
- /56/ Van Olphen, H. 1963.  
"An introduction to clay colloid chemistry. ". Interscience Publishers (John Wiley & Sons) pp 301.
- /57/ Van Straaten, L.M.J.U. and Kuenen, Ph.H., 1958.  
Tidal action as a cause of clay accumulation. *Journal of Sedimentary Petrology* 28 (4), 406-413.
- /58/ Whitehouse, U.G., Jeffrey, L.M., Debbrecht, J.D. 1960.  
Differential settling tendencies of clay minerals in saline waters. In: Swineford (Ed) *Clays and clay minerals*. Proceedings 7th National Conference, Pergamon Press, p 1-79.
- /59/ Yalin, M.S, 1972.  
"Mechanics of Sediment Transport". Pergamon Press Ltd. Headington Hill Hall, Oxford.